

**Research  
Article**

# Dynamics of Offshore Floating Wind Turbines—Model Development and Verification

Jason M. Jonkman\*, National Renewable Energy Laboratory, 1617 Cole Boulevard, Golden, CO 80401-3393, USA

**Key words:**

offshore wind turbine;  
floating;  
model development;  
model verification;  
aero-hydro-servo-elastic analysis

*The vast deepwater wind resource represents a potential to use offshore floating wind turbines to power much of the world with renewable energy. Many floating wind turbine concepts have been proposed, but dynamics models, which account for the wind inflow, aerodynamics, elasticity and controls of the wind turbine, along with the incident waves, sea current, hydrodynamics, and platform and mooring dynamics of the floater, were needed to determine their technical and economic feasibility. This work presents the development of a comprehensive simulation tool for modelling the coupled dynamic response of offshore floating wind turbines and the verification of the simulation tool through model-to-model comparisons. The fully coupled time-domain aero-hydro-servo-elastic simulation tool was developed with enough sophistication to address limitations of previous studies and has features required to perform loads analyses for a variety of rotor-nacelle assembly, tower, support platform and mooring system configurations. The developed hydrodynamics module accounts for linear hydrostatic restoring; non-linear viscous drag; the added-mass and damping contributions from linear wave radiation, including free-surface memory effects; and the incident-wave excitation from linear diffraction in regular or irregular seas. The developed mooring line module is quasi-static and accounts for the elastic stretching of an array of homogenous taut or slack catenary lines with seabed interaction. The hydrodynamics module, the moorings module, and the overall simulation tool were tested by comparing to results of other models, including frequency-domain models. The favourable results of all the verification exercises provided confidence to perform more thorough analyses. Copyright © 2009 John Wiley & Sons, Ltd.*

*Received 10 April 2008; Revised 12 May 2009; Accepted 15 May 2009*

## Introduction

All of the offshore production wind turbines installed to date are on bottom-mounted substructures, and nearly all have been installed in water shallower than 20 m. In contrast, much of the vast offshore wind resource potential in the USA, China, Japan, Norway and many other countries, is available in deeper water. At some water depth, floating support platforms will be the most economical type of support structure.<sup>1</sup>

Numerous floating support platform configurations are possible for offshore wind turbines, particularly considering the variety of mooring systems, tanks and ballast options that are used in the offshore oil and gas

\* Correspondence to: Jason Jonkman, National Renewable Energy Laboratory, 1617 Cole Boulevard, Golden, CO 80401-3393, USA.

E-mail: jason.jonkman@nrel.gov

(O&G) industries. Figure 1 illustrates the three principal concepts, classified in terms of how the designs achieve static stability. The spar-buoy, the tension leg platform (TLP) and the barge concepts use the ballast, the mooring system and the water plane static stability mechanisms, respectively. Hybrid concepts, such as semisubmersibles, which use features from all three classes, are also a possibility.<sup>2</sup>

Because the offshore O&G industries have demonstrated the long-term survivability of offshore floating structures, the technical feasibility of developing offshore floating wind turbines is not in question. Developing cost-effective offshore floating wind turbine designs that are capable of penetrating the competitive energy marketplace, however, will require considerable thought and analysis. Transferring the offshore O&G technology directly to the offshore wind industry without adaptation would not be economical. These economic challenges impart technological challenges,<sup>2</sup> which, in turn, must be addressed through conceptual design and analysis.

Wind turbines are designed and analysed using simulation tools (i.e. design codes) capable of predicting the coupled dynamic response, as well as the extreme and fatigue loads of the system. Land-based wind turbine analysis relies on the use of aero-servo-elastic codes, which incorporate wind-inflow, aerodynamic, control system (servo) and structural-dynamic (elastic) models in the time domain in a coupled simulation environment.

In recent years, a number of these codes have been expanded to include the additional dynamics pertinent to bottom-mounted offshore support structures, including models for incident waves, sea current, hydrodynamics and foundation dynamics of the support structure.<sup>3</sup> However, none of these codes account for hydrodynamic

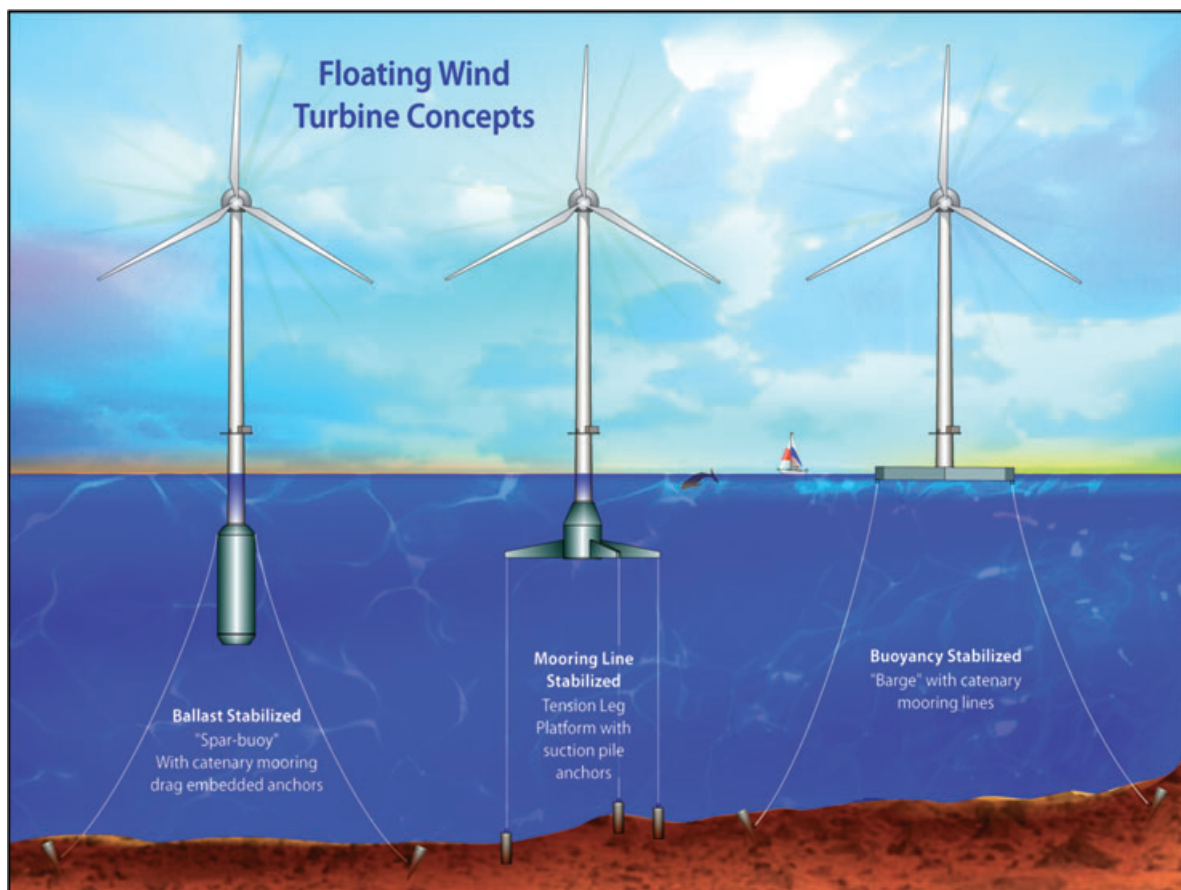


Figure 1. Floating platform concepts for offshore wind turbines

wave-radiation and wave-diffraction loads, as well as mooring system reactions that are important for many of the floating platform concepts.

A number of research studies have assessed the preliminary design of offshore floating wind turbines. Many of these studies<sup>4-7</sup> used linear frequency-domain analysis, which is commonly used in the offshore O&G industries. All of the studies demonstrated the technical feasibility of offshore floating wind turbines by showing that through proper design, the natural frequencies of the floating support platform could be placed where there was little energy in the wave spectrum to ensure that the overall dynamic response was minimized.

One limitation of these linear frequency-domain analyses is that they cannot capture the non-linear dynamic characteristics and transient events that are important considerations in wind turbine analysis. Several other offshore floating wind turbine studies<sup>8-15</sup> have addressed this limitation through the development and application of time-domain dynamics models. These studies showed that platform motions have little effect on power capture and rotor loads; instead, these were dominated by the aerodynamics of the rotor. They also showed, though, that platform motions have a substantial effect on the nacelle and the tower loads, which are dominated by inertia. As a result, the tower would have to be strengthened and the design of the machinery would require a reassessment if the platform motions could not be reduced.

These time-domain studies have other limitations that must also be addressed. Particularly, the dynamic models developed were not general enough to allow analysis of a variety of support platform configurations and were also limited in their capability for the configurations they could model. Moreover, the findings and conclusions drawn by all of these studies must be verified through a rigorous loads analysis.

In light of the limitations of these previous studies, three research objectives were set: (i) develop a comprehensive simulation tool that can model the coupled dynamic response of offshore floating wind turbines; (ii) verify the simulation capability through model-to-model comparisons; and (iii) apply the simulation tool to the integrated loads analysis of promising floating wind turbine concepts. The first two objectives are summarized in this paper. The final objective has been presented for a barge concept in Jonkman,<sup>16</sup> and will be presented for other concepts in future papers. More detail regarding all aspects of the research is available in Jonkman.<sup>16</sup>

In fulfilment of the first objective, the simulation tool was developed with enough sophistication to address the limitations of the previous time- and frequency-domain models of offshore floating wind turbines. In addition, it has the features required to perform an integrated loads analysis for a variety of rotor-nacelle assembly (RNA), tower, support platform and mooring system configurations. The developed simulation tool is a fully coupled aero-hydro-servo-elastic model based in the time domain. By 'aero-hydro-servo-elastic', we mean that aero-servo-elastic models and hydrodynamic models are incorporated in the fully coupled simulation environment. The 'fully coupled' nature of this capability is important for possible follow-on design optimization projects, which would be difficult to carry out without taking the integrated dynamic response into account.

The input data summarized in the Wind Turbine and Floating Platform Model Descriptions section is used for the model verification exercises presented in this paper. The verification exercises fulfil the second objective and were important because they gave confidence in the correctness of the simulation capability. This confidence, in turn, has allowed pursuit of more thorough investigations into the dynamic behaviour of offshore floating wind turbines in fulfilment of the third objective.

## **Overview of Aero-hydro-servo-Elastic Simulation Development**

Limitations with previous time- and frequency-domain studies on offshore floating wind turbines motivated the development of simulation capability for modelling the fully coupled aero-hydro-servo-elastic response of such systems. In developing this capability, it was beneficial to combine the computational methodologies of the land-based wind turbine and of the offshore O&G industries.

Over the past decade, the US Department of Energy's National Renewable Energy Laboratory (NREL) has sponsored the development, verification and validation of comprehensive aero-servo-elastic simulators through

the National Wind Technology Center. The two primary codes are (i) Fatigue, Aerodynamics, Structures and Turbulence (FAST)<sup>17</sup> with AeroDyn;<sup>18</sup> and (ii) MSC.ADAMS® (Automatic Dynamic Analysis of Mechanical Systems) with A2AD (ADAMS-to-AeroDyn)<sup>19</sup> and AeroDyn. FAST and MSC.ADAMS are separate programs that can be run independently to model the structural-dynamic response and control system behaviour of horizontal-axis wind turbines (HAWTs). FAST uses a combined modal and multibody structural-dynamics formulation in the time domain. The more complex MSC.ADAMS code is a commercially available and general-purpose code from MSC Software Corporation that uses a higher fidelity multibody-dynamics formulation in the time domain. It is adaptable for modelling wind turbines through the set of A2AD modules. Note that usage of the term ‘ADAMS’ means ‘MSC.ADAMS with A2AD’ in this paper. The complicated HAWT models possible within ADAMS can be generated through a pre-processor functionality built into the simpler FAST code. To enable the fully coupled aero-servo-elastic modelling of wind turbines, both FAST and ADAMS have been interfaced with the AeroDyn aerodynamic subroutine package for calculating wind turbine aerodynamic forces.

For the offshore O&G industries, the Center for Ocean Engineering at the Massachusetts Institute of Technology has sponsored the development, verification and validation of comprehensive hydrodynamic computer programs capable of analysing the wave interaction and dynamic responses of offshore floating platforms in both the frequency and time domains. The most popular of these programs, Wave Analysis at MIT (WAMIT)<sup>20</sup>, now a commercially available product from WAMIT, Inc., uses a three-dimensional numerical-panel method in the frequency domain to solve the linearized hydrodynamic radiation and diffraction problems for the interaction of surface waves with offshore platforms of arbitrary geometry.

The land-based wind turbine simulation tools FAST with AeroDyn and ADAMS with AeroDyn were upgraded to include the additional dynamic loading and motions representative of offshore floating systems. As will be shown, WAMIT is used in the overall solution. The assumptions inherent in, and the implications of, the new formulations relating to floating support platforms for offshore wind turbines are discussed first. Then, the addition of support platform kinematics and kinetics modelling, the incorporation of support platform hydrodynamics modelling and the inclusion of mooring system modelling into FAST and ADAMS are presented.

The newly developed time-domain hydrodynamics module is called ‘HydroDyn’ because it is to hydrodynamic loading what AeroDyn is to aerodynamic loading in the system.

Equations are extensively used to describe the hydrodynamic and mooring system formulations as they relate to floating support platforms for offshore wind turbines. For conciseness and clarity, the derivations of these equations are not included; it is the form of the equations and the physics behind them that are emphasized (please refer to the associated references for many of the derivations). The distinctions between this model and others used in the offshore wind turbine industry are also emphasized. These distinctions are important because the approach taken in this paper to implement offshore dynamics into wind turbine design codes is substantially different than the approach taken by other modellers who have analysed offshore bottom-mounted and floating wind turbine support structures.

### *Assumptions for the New Model Development*

When adding models for floating wind turbine simulation; including the support platform kinematics, kinetics and hydrodynamics, as well as the mooring system responses, a number of assumptions were invoked in addition to those that were previously inherent in FAST with AeroDyn and ADAMS with AeroDyn.

For the support platform kinematics and kinetics, it is assumed that the floating support platform is represented well as a six-degree-of-freedom (DOF) rigid body with three small rotational displacements (the assumption about small rotations only applies to FAST). As discussed below, the implications of the small-angle assumption are not thought to be critical. Like the load-bearing base plate of the nacelle, the support platform was modelled as a rigid body because it is considered to be so strong and inflexible—at least in relation to the blades and tower—that direct hydro-elastic effects are unimportant. Additionally, it is assumed that the tower is rigidly cantilevered to the support platform. Also, the centre of mass (CM) and centre of buoyancy

(COB) of the support platform (not including the RNA and tower) were assumed to lie along the centreline of the undeflected tower.

The developed mooring system module treats each mooring line quasi-statically. The Mooring System Modelling section presents the development of this model and the implications of its quasi-static characteristic.

The fundamental assumption in the development of the HydroDyn hydrodynamics module was linearization of the classical marine hydrodynamics problem. In the field of marine hydrodynamics, the assumption of linearity signifies many things, three of which are discussed next.

First, linearization of the hydrodynamics problem (i.e. linearization of the non-linear kinematic and dynamic free-surface boundary conditions) implies that the amplitudes of the incident waves are much smaller than their wavelengths. This permits the use of the simplest incident-wave-kinematics theory, which is known as Airy wave theory. This assumption necessarily precludes modelling of steep or breaking waves and the resulting non-linear wave-induced 'slap' and 'slam' loading. Linearization is a reasonable assumption for most waves in deep water and for small-amplitude waves in shallow water. When waves become extreme or propagate towards the shore in shallow water, however, higher-order wave kinematics theories are required. This model neglects high-order wave kinematics theories because they are not compatible with the radiation and diffraction solutions in the model.

Second, linearization implies that the translational displacements of the support platform are small relative to the size of the body (i.e. the characteristic body length). In this way, the hydrodynamics problem can be split into three separate and simpler problems: one for radiation, one for diffraction and one for hydrostatics.

Third, linearization suggests that one can take advantage of the powerful technique of superposition. The hydrodynamics problem uses this technique.

Naturally, linearization of the hydrodynamics problem implies that nonlinear second- or higher-order hydrodynamic effects are not accounted for. The linearized hydrodynamics model, however, has been augmented with the non-linear viscous-drag term from Morison's equation.

These models ignore the potential loading from vortex-induced vibration caused by sea currents. The ancillary effect of the sea current on the radiation and diffraction problems, such as the Doppler-shifted frequency-of-encounter effect,<sup>24</sup> was ignored as well.

Finally, these models ignore the potential loading from floating debris or sea ice, which can be important if the support platform is intended to be used where sea ice is present.

Also note that the classical marine hydrodynamics problem takes advantage of unsteady potential-flow theory to derive the governing equations of fluid motion. This theory assumes that the fluid is incompressible, inviscid and subject only to conservative body forces (i.e. gravity), and that the flow is irrotational.

### **Support Platform Kinematics and Kinetics Modelling**

The first step required in upgrading existing land-based wind turbine simulation tools to make them useful for analysing offshore systems is to introduce DOFs necessary for characterizing the motion of the support platform. For floating systems, it is crucial that all six rigid-body modes of motion of the support platform be included in the development. These include translational surge, sway and heave displacement DOFs, along with rotational roll, pitch and yaw displacement DOFs, as shown in Figure 2. In this figure,  $X, Y, Z$  represents the set of orthogonal axes of an inertial reference frame fixed with respect to the mean location of the support platform, with the  $XY$ -plane designating the still water level (SWL), the  $X$ -axis directed along the nominal wind direction and the  $Z$ -axis directed upward opposite gravity along the centreline of the undeflected tower when the support platform is undisplaced.

Because most of the support platforms that have been proposed for floating wind turbines are more or less axisymmetric, and because there is no hydrodynamic mechanism that will induce yaw moments on such floating bodies, one might question whether the support platform yaw-rotation DOF is necessary. The rotor, however, induces yaw moments that are primarily the result of (i) the aerodynamic loads on the rotor in

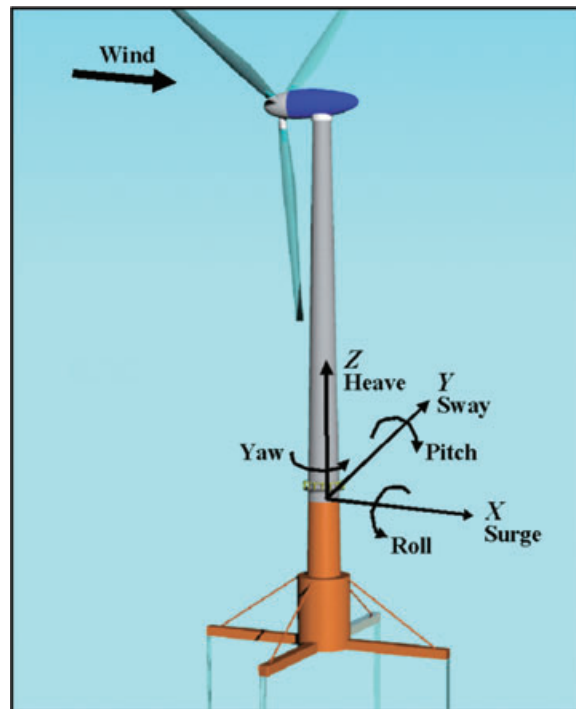


Figure 2. Support platform DOF (source: modified from Withee<sup>9</sup>)

non-uniform or skewed flow; and (ii) the spinning inertia of the rotor combined with pitching motion (whether from support platform pitching or tower deflection), which induces a gyroscopic yaw moment. As implied by (ii), the dynamic coupling between the motions of the support platform and the motions of the supported RNA and tower are crucial in the development of the equations of motion.

In ADAMS, all the dynamic couplings between the motions of the support platform and the motions of the supported RNA and tower were obtained by simply introducing the six-DOF support platform rigid body in the ADAMS model. In FAST, however, these couplings were obtained by introducing the six rigid-body support platform DOFs into the system's equations of motion. While re-deriving the equations of motion, all appropriate terms were incorporated in the derivations of the kinematics expressions for the points and reference frames in the system.

With the assumption that all rotations of the support platform are small, rotation sequence becomes unimportant. Consequently, all the complications of using Euler angles (or the like), where the order of rotation is significant, could be avoided when the equations of motion in FAST were derived and implemented. Take  $x, y, z$  to be the axes of the reference frame resulting from a transformation involving three orthogonal rotations  $(\theta_1, \theta_2, \theta_3)$  about the axes of an original reference frame  $X, Y, Z$ . Using the first-order small-angle approximations for the sine and cosine functions, as well as neglecting terms of higher order in the Taylor series expansion, the standard Euler-angle transformation<sup>21</sup> relating the original and transformed reference frames simplifies to

$$\begin{Bmatrix} x \\ y \\ z \end{Bmatrix} \approx \begin{bmatrix} 1 & \theta_3 & -\theta_2 \\ -\theta_3 & 1 & \theta_1 \\ \theta_2 & -\theta_1 & 1 \end{bmatrix} \begin{Bmatrix} X \\ Y \\ Z \end{Bmatrix} \quad (1)$$

In this equation, the approximation sign ( $\approx$ ) is used in place of an equal symbol ( $=$ ) because the resulting transformation matrix is not orthonormal beyond first order when the small-angle approximations are used.

This implies that the transformed reference frame is not made up of a set of mutually orthogonal axes. Because using axes that are not mutually orthogonal can lead to inaccuracies that propagate in the dynamic-response calculations, a correction to the transformation matrix in equation (1) was invoked to ensure that it remained orthonormal. From matrix theory,<sup>22</sup> we know that the closest orthonormal matrix to a given matrix, in the sense of the Frobenius norm, is  $[U][V]^T$ , where  $[U]$  and  $[V]$  are the matrices of eigenvectors inherent in the singular-value decomposition of the given matrix and the symbol  $^T$  represents a matrix transpose. By performing these operations, the correct transformation expression was found to be

$$\begin{Bmatrix} x \\ y \\ z \end{Bmatrix} = \begin{bmatrix} \frac{\theta_1^2 \sqrt{1+\theta^2} + \theta_2^2 + \theta_3^2}{\theta^2 \sqrt{1+\theta^2}} & \frac{\theta_3 \theta^2 + \theta_1 \theta_2 (\sqrt{1+\theta^2} - 1)}{\theta^2 \sqrt{1+\theta^2}} & \frac{-\theta_2 \theta^2 + \theta_1 \theta_3 (\sqrt{1+\theta^2} - 1)}{\theta^2 \sqrt{1+\theta^2}} \\ \frac{-\theta_3 \theta^2 + \theta_1 \theta_2 (\sqrt{1+\theta^2} - 1)}{\theta^2 \sqrt{1+\theta^2}} & \frac{\theta_1^2 + \theta_2^2 \sqrt{1+\theta^2} + \theta_3^2}{\theta^2 \sqrt{1+\theta^2}} & \frac{\theta_1 \theta^2 + \theta_2 \theta_3 (\sqrt{1+\theta^2} - 1)}{\theta^2 \sqrt{1+\theta^2}} \\ \frac{\theta_2 \theta^2 + \theta_1 \theta_3 (\sqrt{1+\theta^2} - 1)}{\theta^2 \sqrt{1+\theta^2}} & \frac{-\theta_1 \theta^2 + \theta_2 \theta_3 (\sqrt{1+\theta^2} - 1)}{\theta^2 \sqrt{1+\theta^2}} & \frac{\theta_1^2 + \theta_2^2 + \theta_3^2 \sqrt{1+\theta^2}}{\theta^2 \sqrt{1+\theta^2}} \end{bmatrix} \begin{Bmatrix} X \\ Y \\ Z \end{Bmatrix} \quad (2)$$

where  $\theta^2 = \theta_1^2 + \theta_2^2 + \theta_3^2$ .

When applied to the support platform,  $x, y, z$  represents the set of orthogonal axes of the body-fixed reference frame within the support platform and  $\theta_1, \theta_2, \theta_3$  are the roll, pitch and yaw rotations of the support platform about the axes of the inertial reference frame (i.e.  $X, Y, Z$ ). The origin of  $x, y, z$  is called the platform reference point and is the location in the platform about which the support platform DOFs are defined. It is also the point at which the hydrodynamic loads and mooring system loads are applied to the support platform. Similar labelling of  $x, y, z$  and  $X, Y, Z$  is used when applying equation (2) to relate a reference frame that is oriented with an element of a deflected blade (or tower) to the reference frame fixed in the root of the blade (or tower)—in this case, the rotations are the flap, lag and twist slopes of the blade (or tower) element.

In FAST, equation (2) has been implemented instead of equation (1) for all transformations relating the support platform to the inertial frame, all transformations relating the deflected tower elements to the tower base, and all transformations relating the deflected blade elements to the root of the blade. Although these results are not shown here, it has been demonstrated that incorporating equation (2) in FAST instead of equation (1) leads to dynamic responses that are in much better agreement with responses obtained from ADAMS, which uses Euler angles, especially as the magnitude of the angles increases. The dynamic responses are more accurate when equation (2) is used in place of equation (1) because such transformation matrices get multiplied in series when determining the orientation of subsystems far along the load path away from the inertial frame, such as in a tower or blade element. Errors in a single transformation matrix are compounded when multiplied together. If the wind turbine was very rigid, the correction would not be necessary.

The transformation expression of equation (2) still loses considerable accuracy when any of the angles greatly exceed  $20^\circ$ . This threshold, however, should be adequate for support platform designs suitable for floating wind turbines because with large inclinations of the tower and machinery: (i) the steady and dynamic loads would be severe; (ii) the energy capture from the wind would diminish; and (iii) the access intervals for maintenance personnel would be limited.

Kane's dynamics<sup>23</sup> were used to derive the equations of motion used in FAST. Although it was a long and tedious process, there was no particular difficulty in deriving the FAST system's equations of motion (which are not presented here). To summarize, first the kinematics expressions were derived and the partial velocity vectors utilized by Kane's dynamics were established. These, along with expressions for the generalized active and inertia forces, established the kinetics and led systematically to the complete nonlinear time-domain equations of motion of the coupled RNA, tower and support platform system. The kinetics expressions for the support platform included contributions from platform mass and inertia, gravity, hydrodynamics and the reaction loads of the mooring system.

Once derived, the complete nonlinear time-domain equations of motion of the coupled RNA, tower, and support platform system are of the general form:

$$M_{ij}(q, u, t)\ddot{q}_j = f_i(q, \dot{q}, u, t) \quad (3)$$

where  $M_{ij}$  is the  $(i,j)$  component of the inertia mass matrix, which depends non-linearly on the set of system DOFs ( $q$ ), control inputs ( $u$ ) and time ( $t$ );  $\ddot{q}_j$  is the second time derivative of DOF  $j$ ; and  $f_i$  is the component of the forcing function associated with DOF  $i$ . The forcing function,  $f_i$ , depends nonlinearly on the set of system DOFs and their first time derivatives ( $q$  and  $\dot{q}$  respectively), as well as the set of control inputs ( $u$ ) and time ( $t$ ), and is positive in the direction of positive motion of DOF  $i$ . Equation (3) uses Einstein notation, which implies that when the same subscript appears in multiple variables in a single term, there is a sum of all of the possible terms. Subscripts  $i$  and  $j$  range from one to the total number of DOFs in the model.

Built into equation (3) are the applied aerodynamic and gravitational loads, the behaviour of the control and protection systems, and the structural dynamics of the wind turbine. The latter contribution includes the elasticity of the RNA and tower, along with the newly added dynamic coupling between their motions and the motions of the support platform. Up to this point, the loads unique to floating wind turbines (other than the inertia loads of the support platform), including hydrodynamic loads and mooring system loads, have only been considered heuristically as additional loads acting on the support platform. Naturally, when hydrodynamic loading on the support platform is present, hydrodynamic-impedance forces—including the influence of added mass—are important. To ensure, then, that the equations of motion were not implicit (i.e., to avoid  $f_i$  depending on  $\ddot{q}$ ), the additional loads acting on the support platform that are unique to floating wind turbines (i.e. the loads other than what are transmitted from the RNA, tower and the weight of the support platform) were split into two components: an impulsive added-mass component summing with  $M_{ij}$  and the rest of the load adding to  $f_i$ . In other words, the total load acting on the support platform from hydrodynamics and moorings,  $F_i^{Platform}$ , was written as follows:

$$F_i^{Platform} = -A_{ij}\ddot{q}_j + F_i^{Hydro} + F_i^{Lines} \quad (4)$$

where  $A_{ij}$  is the  $(i,j)$  component of the impulsive hydrodynamic-added-mass matrix to be summed with  $M_{ij}$ ,  $F_i^{Hydro}$  is the  $i$ th component of the applied hydrodynamic load on the support platform associated with everything but  $A_{ij}$  and  $F_i^{Lines}$  is the  $i$ th component of the applied load on the support platform from the contribution of all mooring lines.  $F_i^{Hydro}$  and  $F_i^{Lines}$  are both included with the rest of the forcing function,  $f_i$ , in equation (3). In equation (4), subscripts  $i$  and  $j$  range from 1 to 6; one for each support platform DOF (1 = surge, 2 = sway, 3 = heave, 4 = roll, 5 = pitch, 6 = yaw). The forms of the hydrodynamic impulsive-added-mass and hydrodynamic-forcing terms are discussed in the Support Platform Hydrodynamics Modelling section, and the term associated with the mooring lines is discussed in the Mooring System Modelling section.

### Support Platform Hydrodynamics Modelling

Hydrodynamics are included within computer simulation programs by incorporating a suitable combination of incident-wave kinematics and hydrodynamic loading models. Hydrodynamic loads result from the integration of the dynamic pressure of the water over the wetted surface of a floating platform. These loads include contributions from inertia (added mass) and linear drag (radiation), buoyancy (restoring), incident-wave scattering (diffraction), sea current and nonlinear effects.

The following subsections discuss the true linear hydrodynamic-loading equations in the time domain, taking advantage of the assumptions outlined earlier. By ‘true linear hydrodynamic-loading equations’, we mean that these equations satisfy the linearized governing boundary-value problems exactly, without restriction on platform size, shape or manner of motion (other than those required for the linearization assumption to hold). These equations are compared and contrasted with alternative hydrodynamic formulations, which are routinely used in the offshore industry but contain restrictions that limit their direct application to the analysis of many offshore floating wind turbines. The parts of all the formulations are brought together in developing the Hydro-

Dyn support platform hydrodynamics module for offshore floating wind turbines. Figure 3 summarizes the HydroDyn calculation procedure.

*The True Linear Hydrodynamic Model in the Time Domain*

In linear hydrodynamics, the hydrodynamics problem can be split into three separate and simpler problems: one for radiation, one for diffraction and one for hydrostatics.<sup>24,25</sup> The radiation problem seeks to find the loads on a floating platform when the body is forced to oscillate in its various modes of motion and no incident surface waves are present. The resulting radiation loads are brought about as the body radiates waves away from itself (i.e. it generates outgoing waves) and include contributions from added mass and from wave-radiation damping. The diffraction problem seeks to find the loads on a floating platform when the body is fixed at its mean position (no motion) and incident surface waves are present and scattered by the body. The diffraction loads are the result of the undisturbed pressure field (Froude-Kriloff) and wave scattering. The hydrostatics problem is elementary, but is nevertheless crucial in the overall behaviour of a floating platform.

The total load from hydrodynamics and moorings acting on the support platform of an offshore floating wind turbine is in the form of equation (4). In the true linear hydrodynamics problem, the term  $F_i^{Hydro}$  in equation (4) is of the form shown in equation (5).<sup>26,27</sup> The terms of this equation are discussed separately.

$$F_i^{Hydro} = F_i^{Waves} + \rho g V_0 \delta_{i3} - C_{ij}^{Hydrostatic} q_j - \int_0^t K_{ij}(t - \tau) \dot{q}_j(\tau) d\tau \tag{5}$$

The first term on the right-hand side of equation (5),  $F_i^{Waves}$ , represents the total excitation load on the support platform from incident waves and is closely related to the wave elevation,  $\zeta$ . As background, Airy wave theory<sup>24,25</sup> describes the kinematics of regular waves, whose periodic elevation is represented as a sinusoid propagating at a single amplitude and frequency (period) or wavelength (Airy wave theory also describes how the undisturbed fluid-particle velocities and accelerations decay exponentially with depth). Irregular or random waves that represent various stochastic sea states are modelled as the summation or superposition of multiple

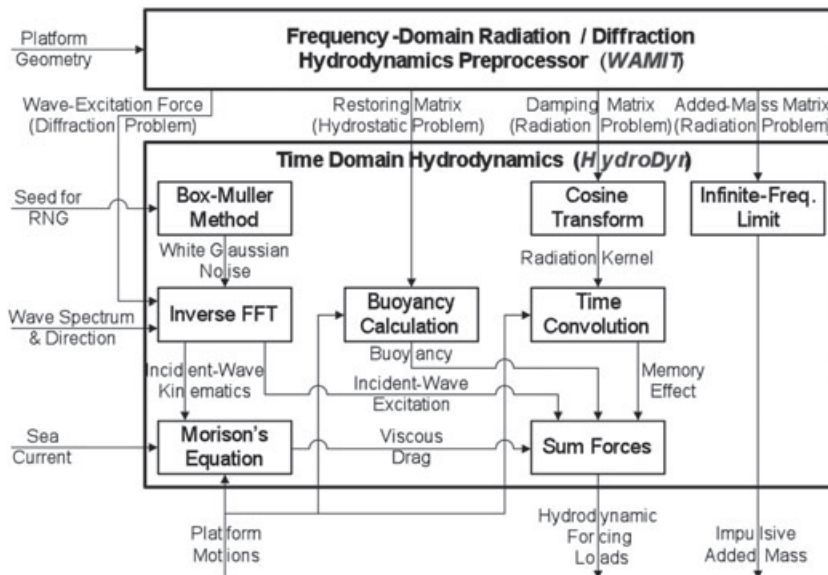


Figure 3. Summary of the HydroDyn calculation procedure

wave components, as determined by an appropriate wave spectrum. Expressions for  $\zeta$  and  $F_i^{Waves}$  are given by:

$$\zeta(t)|_{t=n\Delta t} = \frac{1}{N} \sum_{k=-\frac{N}{2}+1}^{\frac{N}{2}} W[k] \sqrt{\frac{2\pi}{\Delta t} S_{\zeta}^{2-Sided}(\omega)} \Big|_{\omega=k\Delta\omega} e^{j\frac{2\pi kn}{N}} \quad \text{for } n=0, 1, \dots, N-1 \quad (6)$$

and

$$F_i^{Waves}(t)|_{t=n\Delta t} = \frac{1}{N} \sum_{k=-\frac{N}{2}+1}^{\frac{N}{2}} W[k] \sqrt{\frac{2\pi}{\Delta t} S_{\zeta}^{2-Sided}(\omega)} \Big|_{\omega=k\Delta\omega} X_i(\omega, \beta)|_{\omega=k\Delta\omega} e^{j\frac{2\pi kn}{N}} \quad \text{for } n=0, 1, \dots, N-1 \quad (7)$$

Equations (6) and (7) are inverse discrete Fourier transforms, where  $j$  is the imaginary number,  $\sqrt{-1}$ ,  $n$  is the discrete-time-step counter,  $k$  is the discrete-frequency-step counter and  $N$  is the number of discrete steps.  $N$  is related to the time step,  $\Delta t$ , and frequency step,  $\Delta\omega$ , by the sampling theorem  $N = \frac{2\pi}{\Delta t \Delta\omega} = \frac{t_{max}}{\Delta t} = \frac{2\omega_{max}}{\Delta\omega}$ , where  $t_{max}$  is the total analysis time and  $\omega_{max}$  is the highest (in magnitude) frequency considered.<sup>28</sup>  $S_{\zeta}^{2-Sided}$  in equations (6) and (7) represents the desired (target) two-sided power spectral density (PSD) of the wave elevation per unit time (i.e. the two-sided wave spectrum), which depends on the frequency of the incident waves,  $\omega$ .  $W[k]$  represents the discrete Fourier transform of a realization of a white Gaussian noise discrete-time-series process with zero mean and unit variance (i.e. the so-called ‘standard normal distribution’). This realization is used to ensure that the individual wave components have a random phase and that the instantaneous wave elevation is normally (i.e. Gaussian-) distributed with zero mean and with a variance, on average, equal to  $\sigma_{\zeta}^2 = \int_{-\infty}^{\infty} S_{\zeta}^{2-Sided}(\omega) d\omega$ . The same realization is used in the computation of the wave elevation and in the computation of the incident-wave force.  $X_i(\omega, \beta)$  is a complex-valued array that represents the wave-excitation force on the support platform normalized per unit wave amplitude; the imaginary components permit the force to be out of phase with the wave elevation. This force depends on the geometry of the support platform, and the frequency and direction of the incident wave,  $\omega$  and  $\beta$ , respectively, and it is discussed further later. The incident-wave-propagation heading direction,  $\beta$ , which is zero for waves propagating along the positive  $X$ -axis of the inertial frame, and positive for positive rotations about the  $Z$ -axis, is an input to the model. This allows for the simulation of conditions in which the wind and wave directions are not aligned.

Equation (7) for the incident-wave-excitation force is very similar to equation (6) for the incident-wave elevation—the only difference is the inclusion of the normalized wave-excitation force complex transfer function,  $X_i$ . This follows directly from linearization of the diffraction problem. Superposition of the diffraction problem implies that (i) the magnitude of the wave-excitation force from a single wave is linearly proportional to the wave amplitude; and (ii) the wave-excitation force from multiple superimposed waves is the same as the sum of the wave-excitation forces produced by each individual wave component. The inverse discrete Fourier transforms in HydroDyn are implemented using computationally efficient fast Fourier transform (FFT) routines.<sup>29</sup>

The realization of the white Gaussian noise process in HydroDyn is calculated using the Box-Muller method,<sup>30</sup> which considers not only a uniformly-distributed random phase, but also a normally distributed amplitude. The normally distributed amplitude ensures that the resulting wave elevation is Gaussian-distributed, but causes the actual wave spectrum and variance to vary among realizations (this is why the variance of the resulting wave elevation was earlier referred to as ‘on average’). To ensure that the wave spectrum and variance remains constant for every realization requires that one consider only random phase variations among the individual wave components—but then the instantaneous wave elevation would only be Gaussian-distributed with an infinite number of wave components.). The normally distributed amplitude is optional in HydroDyn and can be used to randomly deviate from the (most likely idealized) target wave spectrum.

The second and third terms on the right-hand side of equation (5) combined,  $\rho g V_0 \delta_{i3} - C_{ij}^{Hydrostatic} q_j$ , represent the load contribution from hydrostatics as implemented in HydroDyn. Here,  $\rho$  is the water density,  $g$  is the gravitational acceleration constant,  $V_0$  is the displaced volume of fluid when the support platform is in its undisplaced position,  $\delta_{i3}$  is the  $(i,3)$  component of the Kronecker–Delta function (i.e. identity matrix) and  $C_{ij}^{Hydrostatic}$  is the  $(i,j)$  component of the linear hydrostatic-restoring matrix from the effects of water-plane area and the COB. The hydrostatic loads are independent of the incident and outgoing waves from the diffraction and radiation problems, respectively.

The first of these terms,  $\rho g V_0 \delta_{i3}$ , represents the buoyancy force from Archimedes’ principle; that is, it is the force directed vertically upward and equal to the weight of the displaced fluid when the support platform is in its undisplaced position. This term is non-zero only for the vertical heave-displacement DOF of the support platform (DOF  $i = 3$ ) because the COB of the platform is assumed to lie on the centreline of the undeflected tower (or  $z$ -axis of the platform). In the field of naval architecture and in the analysis of large offshore O&G platforms, the term  $\rho g V_0 \delta_{i3}$  is not often found in the equations of motion because it cancels with the weight in air of the floating body and the weight in water of the mooring system. Because the location of the CM of the floating wind turbine continually changes as a result of RNA and tower flexibility, however, it was important to separate out the individual contributions of gravity. These contributions are RNA, tower and support platform weight, weight in water of the mooring system and buoyancy. The weights of the RNA, tower and support platform are inherent in the  $f_i$  term of equation (3).

The second of the hydrostatic terms,  $-C_{ij}^{Hydrostatic} q_j$ , represents the change in the hydrostatic force and moment resulting from the effects of the water-plane area and the COB as the support platform is displaced. The water-plane area of the support platform in its undisplaced position,  $A_0$ , affects the hydrostatic load because the displaced volume of the fluid changes with changes in the support platform displacement ( $q_j$ ). Similarly, the body-fixed vertical location of the COB of the support platform,  $z_{COB}$ , affects the hydrostatic load because the vector position of the COB also changes with platform displacement and because the cross product of the buoyancy force with the vector position of the COB produces a hydrostatic moment about the support platform reference point. The only non-zero components of  $C_{ij}^{Hydrostatic}$  are (3,3), (4,4), (5,5), (3,5) and (5,3) when the body-fixed  $xz$ -plane of the submerged portion of the support platform is a plane of symmetry:<sup>24</sup>

$$C_{ij}^{Hydrostatic} = \begin{bmatrix} 0 & 0 & 0 & 0 & 0 & 0 \\ 0 & 0 & 0 & 0 & 0 & 0 \\ 0 & 0 & \rho g A_0 & 0 & -\rho g \iint_{A_0} x dA & 0 \\ 0 & 0 & 0 & \rho g \iint_{A_0} y^2 dA + \rho g V_0 z_{COB} & 0 & 0 \\ 0 & 0 & -\rho g \iint_{A_0} x dA & 0 & \rho g \iint_{A_0} x^2 dA + \rho g V_0 z_{COB} & 0 \\ 0 & 0 & 0 & 0 & 0 & 0 \end{bmatrix} \quad (8)$$

If the body-fixed  $yz$ -plane of the submerged portion of the support platform is also a plane of symmetry, the (3,5) and (5,3) components of  $C_{ij}^{Hydrostatic}$  are also zero. Equation (8) clearly demonstrates how hydrostatics provides restoring only for roll, pitch and heave motions; restoring in the other modes of motion must be realized by the mooring system.

The wave-radiation loads include contributions from hydrodynamic added mass and damping. Because the radiation problem has been separated from the diffraction problem, the wave-radiation loads are independent of the incident waves.

In equation (4), the impulsive hydrodynamic-added-mass components,  $A_{ij}$ , represent the force mechanism proportional to the acceleration of the support platform in the time-domain radiation problem. In particular, the  $(i,j)$  component represents the hydrodynamic force in the direction of DOF  $i$  resulting from the integration (over the wetted surface of the support platform) of the component of the outgoing-wave pressure field induced

by, and proportional to, a unit acceleration of the  $j$ th DOF of the support platform. Like the body (inertia) mass matrix, the impulsive hydrodynamic-added-mass matrix is symmetric. Unlike the inertia mass matrix, and depending on the shape of the support platform, the impulsive hydrodynamic-added-mass matrix may contain off-diagonal components that couple modes of motion that cannot be coupled through body inertia.

The last term in equation (5),  $-\int_0^t K_{ij}(t-\tau)\dot{q}_j(\tau)d\tau$ , is a convolution integral representing an additional load contribution from wave-radiation that is not accounted for in  $A_{ij}$ . In this expression,  $\tau$  is a dummy variable with the same units as the simulation time,  $t$ , and  $K_{ij}$  is the  $(i,j)$  component of the matrix known as the wave-radiation-retardation kernel. In the radiation problem, the free surface brings about the existence of memory effects, denoting that the wave-radiation loads depend on the history of motion for the support platform.

The meaning of the wave-radiation-retardation kernel is found by considering a unit impulse in support platform velocity. Specifically, the  $(i,j)$  component of the kernel,  $K_{ij}(t)$ , represents the hydrodynamic force at time  $t$  in the direction of DOF  $i$  resulting from a unit impulse in velocity at time zero of DOF  $j$ . The wave-radiation-retardation kernel, consequently, is commonly referred to as the impulse-response functions of the radiation problem. An impulse in support platform velocity causes a force at all subsequent time because the resulting outgoing free-surface waves induce a pressure field within the fluid domain that persists for as long as the waves radiate away. As in the diffraction problem, the convolution integral in the radiation problem follows directly from the assumption of linearity. According to Ogilvie<sup>27</sup> (p. 33), superposition of the radiation problem implies that if the support platform ‘experiences a succession of impulses, its response at any time is assumed to be the sum of its responses to the individual impulses, each response being calculated with an appropriate time lag from the instant of the corresponding impulse. These impulses can be considered as occurring closer and closer together, until finally one integrates the responses, rather than summing them’.

Using a technique that could be labelled ‘convolution by parts’ (instead of ‘integration by parts’) and assuming zero-valued initial conditions, the convolution integral in the radiation problem can be rewritten as follows:<sup>31</sup>

$$-\int_0^t K_{ij}(t-\tau)\dot{q}_j(\tau)d\tau = -\int_0^t L_{ij}(t-\tau)\ddot{q}_j(\tau)d\tau \quad (9)$$

where the convolution kernels,  $K_{ij}$  and  $L_{ij}$ , are related by

$$K_{ij}(t) = \frac{d}{dt} L_{ij}(t) \quad (10)$$

Equation (9) highlights the elusive nature of the memory effect in the radiation problem—that both acceleration-dependent (added-mass) and velocity-dependent (damping) forces are captured by the convolution term. The impulsive hydrodynamic-added-mass matrix and retardation kernels from the radiation problem are discussed further later.

The HydroDyn module implements a numerical convolution in the time domain to capture the memory effect directly. The velocity formulation from the left-hand side of equation (9) was chosen for implementation because it is more convenient than the acceleration formulation from the right-hand side. The latter would lead to an implicit formulation of the time-domain equations of motion for the coupled RNA, tower and support platform system. As demonstrated with the verification exercises that are presented later, the memory effect, in general, decays to zero after a certain amount of lapsed time. Because of this, HydroDyn is enabled to truncate the numerical convolution after a user-specified amount of time. This allows for faster calculations of the memory effect.

### Comparison to Alternative Hydrodynamic Models

The true linear hydrodynamic-loading equations were discussed above. Alternative hydrodynamics formulations, however, are routinely used in the offshore industry. The two most common alternatives are the frequency-domain representation and Morison’s representation.

The frequency-domain representation is most aligned with how marine hydrodynamics is taught in the classroom and presented in textbooks. For instance, the frequency-domain representation is the hydrodynamics formulation most emphasized in Faltinsen<sup>24</sup> and Newman,<sup>25</sup> which are popular textbooks in ocean-engineering education. The presentation here summarizes these references.

In the time-domain representation of the frequency-domain problem, equation (4)—the total load from hydrodynamics and moorings acting on the support platform of an offshore floating wind turbine—is replaced with

$$F_i^{Platform}(t) = -A_{ij}(\omega)\ddot{q}_j + Re\{AX_i(\omega, \beta)e^{j\omega t}\} - [C_{ij}^{Lines} + C_{ij}^{Hydrostatic}]q_j - B_{ij}(\omega)\dot{q}_j + \rho g V_0 \delta_{i3} + F_i^{Lines,0} \quad (11)$$

where  $A$  is the amplitude of a regular incident wave of frequency  $\omega$  and direction  $\beta$ ,  $F_i^{Lines,0}$  and  $C_{ij}^{Lines}$  are contributions from the mooring system (discussed in the Mooring System Modelling section), and  $A_{ij}(\omega)$  and  $B_{ij}(\omega)$  are the  $(i,j)$  components of the hydrodynamic-added-mass and -damping matrices, which are frequency dependent.  $Re\{\}$  denotes the real value of the argument; the only complex-valued terms in equation (11) are the normalized wave-excitation force,  $X_i$ , and the harmonic exponential,  $e^{j\omega t}$ .

The frequency-domain hydrodynamics problem makes use of the same assumptions used in the true linear hydrodynamics formulation. There are additional requirements, however. The incident wave must propagate at a single amplitude, frequency and direction (i.e. the incident wave is a regular wave), and the platform motions must be oscillatory at the same frequency as the incident wave.

Even though the frequency-domain formulation cannot be directly applied to the transient analysis of offshore floating wind turbines, where non-linear effects, transient behaviour and irregular sea states are important, the solution to the frequency-domain problem is valuable in determining the parameters used in the true linear hydrodynamic-loading equations. For instance, the solution to the frequency- (and direction-) dependent wave-excitation force,  $X_i(\omega, \beta)$ , is needed not only in the frequency-domain solution, but also in the time-domain formulation of the linearized diffraction problem in equation (7). Equally important is the relationship between  $A_{ij}(\omega)$  and  $B_{ij}(\omega)$  from the frequency-domain solution and  $A_{ij}$  and  $K_{ij}(t)$  from the time-domain formulation of the linearized radiation problem. By forcing a particular mode of motion of the support platform to be sinusoidal in the true linear hydrodynamics formulation, and comparing the resulting expression to the time-domain representation of the frequency-domain problem, Ogilvie<sup>27</sup> shows that

$$A_{ij}(\omega) = A_{ij} - \frac{1}{\omega} \int_0^{\infty} K_{ij}(t) \sin(\omega t) dt \quad (12)$$

and

$$B_{ij}(\omega) = \int_0^{\infty} K_{ij}(t) \cos(\omega t) dt \quad (13)$$

The  $A_{ij}$  term on the right-hand side of equation (12) represents the impulsive hydrodynamic-added-mass matrix from equation (4). Note that equation (13) is valid only when the ancillary effects of sea current or forward speed are ignored in the radiation problem (as assumed); though not given here, a slightly different expression exists when these effects are important.

Equations (12) and (13) highlight the interdependence between the hydrodynamic added mass and damping. Equation (9) alluded to their relationship, which is discussed more in Ogilvie.<sup>27</sup>

Because the radiation-retardation kernel,  $K_{ij}(t)$ , may be assumed to be of finite energy, application of the Riemann–Lebesgue lemma to equation (13) reveals that the infinite-frequency limit of  $B_{ij}(\omega)$  is zero. Similarly, the infinite-frequency limit of equation (12) yields

$$A_{ij} = \lim_{\omega \rightarrow \infty} A_{ij}(\omega) = A_{ij}(\infty) \quad (14)$$

Thus, the appropriate impulsive added-mass matrix to be used in the true linear hydrodynamic-loading equations does not depend on frequency, but is the infinite-frequency limit of the frequency-dependent

added-mass matrix, represented here as  $A_{ij}(\infty)$ . This limit does, in general, exist for three-dimensional bodies.

Through application of Fourier-transform techniques and equation (14), equation (12) and (13) can be rearranged to show that

$$K_{ij}(t) = -\frac{2}{\pi} \int_0^{\infty} \omega [A_{ij}(\omega) - A_{ij}(\infty)] \sin(\omega t) d\omega \quad (15a)$$

or

$$K_{ij}(t) = \frac{2}{\pi} \int_0^{\infty} B_{ij}(\omega) \cos(\omega t) d\omega \quad (15b)$$

As a corollary to the interdependence between added mass and damping discussed previously, equation (15) shows that the radiation-retardation kernel depends on both added mass and damping. Once the solution of the frequency-domain radiation problem has been found, one of these expressions can be used to find the wave-radiation-retardation kernel to be used in the true linear hydrodynamic-loading equations. The HydroDyn module implements the cosine transform of Eq. (15b) to find  $K_{ij}(t)$  from  $B_{ij}(\omega)$  using a computationally efficient FFT routine.<sup>29</sup>

Because the frequency-domain approach is so often used in analyses in the offshore O&G industries, many computer codes are available for solving the frequency-domain hydrodynamics problem. The WAMIT code is the most popular of these. The hydrodynamics formulation in HydroDyn is applied identically regardless of how the frequency-domain radiation and diffraction problems are first solved. This is because the frequency-dependent hydrodynamic-added-mass and -damping matrices ( $A_{ij}$  and  $B_{ij}$ ) and wave-excitation force ( $X_i$ ) are simply inputs to HydroDyn.

Morison's representation is widely used in the analysis of bottom-mounted offshore wind turbines.<sup>3</sup> Morison's representation, in conjunction with strip theory, can be used to compute the linear wave loads and nonlinear viscous-drag loads in a straightforward manner, mostly for slender cylinders. In hydrodynamic strip theory, as in blade-element/momentum theory for rotor aerodynamics, the structure is split into a number of elements or strips, where two-dimensional properties (added-mass and viscous-drag coefficients in the case of Morison's hydrodynamics) are used to determine the overall three-dimensional loading on the structure.<sup>24</sup>

If strip theory were to be used, the hydrodynamic components of the load acting on a vertical cylindrical support platform—the hydrodynamic components of  $F_i^{Platform}$  in equation (4)—would be found by integrating over the length of the cylinder the loads acting on each strip,  $dF_i^{Platform}$ . In the relative form of Morison's representation, the hydrodynamic components of equation (4) for the surge and sway modes of motion ( $I = 1$  and 2) are replaced with Morison's equation:<sup>24,25</sup>

$$\begin{aligned} dF_i^{Platform}(t, z) = & -C_A \rho \left( \frac{\pi D^2}{4} dz \right) \ddot{q}'_i(z) + (1 + C_A) \rho \left( \frac{\pi D^2}{4} dz \right) a_i(t, 0, 0, z) \\ & + \frac{1}{2} C_D \rho (D dz) \underbrace{[v_i(t, 0, 0, z) - \dot{q}'_i(z)] \sqrt{[v_1(t, 0, 0, z) - \dot{q}'_1(z)]^2 + [v_2(t, 0, 0, z) - \dot{q}'_2(z)]^2}}_{dF_i^{Viscous}(t, z)} \quad \text{for } i = 1 \text{ or } 2 \end{aligned} \quad (16a)$$

In this equation,  $D$  is the diameter of the cylinder,  $dz$  is the length of the differential strip of the cylinder,  $C_A$  and  $C_D$  are the hydrodynamic-added-mass and viscous-drag coefficients, and  $dF_i^{Viscous}$  is the viscous-drag load acting on the strip of the cylinder.  $\dot{q}'_i(z)$  and  $\ddot{q}'_i(z)$  are the components of the translational velocity and acceleration of the cylinder at height  $z$  in the surge ( $i = 1$ ) and sway ( $i = 2$ ) directions, which are related to the rigid-body support platform DOFs by the time derivatives of  $q'_1 = q_1 + q_5 z$  and  $q'_2(z) = q_2 - q_4 z$ .  $v_i$  and  $a_i$  are

the components of the undisturbed fluid-particle velocity and acceleration in the direction of DOF  $i$ . ( $v_i$  and  $a_i$ , including their arguments, are spelled out in Jonkman<sup>16</sup>).

Using strip theory, expressions similar to equation (16a) can be written for the roll and pitch moments ( $i = 4$  and  $5$ ). Because a cylinder is axisymmetric, the yaw moment ( $i = 6$ ) is zero, and because Morison's equation does not account for end effects, the heave force ( $i = 3$ ) is also zero (when Morison's equation is used to calculate the hydrodynamic loads on an offshore floating wind turbine, the hydrostatic restoring must be added as a separate load). These expressions are all given in equation (16b):

$$dF_i^{Platform}(t, z) = \begin{cases} 0 & \text{for } i = 3 \\ -dF_2^{Platform}(t, z)z & \text{for } i = 4 \\ dF_1^{Platform}(t, z)z & \text{for } i = 5 \\ 0 & \text{for } i = 6 \end{cases} \quad (16b)$$

By comparing equation (16) with the true linear hydrodynamic-loading equations, it can be seen that Morison's representation assumes that viscous drag dominates the damping such that wave-radiation damping can be ignored. This assumption is valid only if the diameter and motions of the cylinder are very small (i.e. it is most appropriate when the cylinder is slender, bottom-mounted and very rigid). The viscous-drag load is not part of the linear hydrodynamic-loading equations because the viscous-drag load is proportional to the square of the relative velocity between the fluid particles and the platform. Nevertheless, the linear hydrodynamic-loading equations in HydroDyn are augmented by including the nonlinear viscous-drag term from Morison's equation as presented in equation (16). The viscous-drag term was included by assigning an effective platform diameter ( $D$ ) and by integrating  $dF_i^{Viscous}$  over the draft of the support platform to find the total viscous-drag load,  $F_i^{Viscous}$ . This effect was included because (i) it was relatively easy to add; (ii) it allowed the influence of sea current to be incorporated; and (iii) it can be an important source of hydrodynamic damping in some situations. To include the influence of sea current generated by winds, tides, and thermal gradients in HydroDyn, a steady, depth-varying current velocity is vectorally combined with the surface-wave-particle velocity when computing the viscous-drag term from Morison's equation.

By comparing equation (16) with the true linear hydrodynamic-loading equations, it is also seen that Morison's representation ignores off-diagonal terms in the added-mass matrix other than those that directly couple the motions between surge and pitch and sway and roll. It may do this because a cylinder is axisymmetric, which ensures that there is no other added-mass-induced coupling between modes of motion.

Morison's representation also takes advantage of G. I. Taylor's long-wavelength approximation<sup>26,27</sup> to simplify the diffraction problem (i.e. the cylinder must be slender, with  $D$  much smaller than the wavelength). This approximation is how the second term in equation (16a) for the wave-excitation force can be expressed in terms of the added-mass coefficient and the undisturbed fluid-particle acceleration along the centreline of the cylinder.

These assumptions inherent in Morison's representation explain why it is not applicable (except for the viscous-drag term) for the analysis of many of the proposed platform concepts for offshore floating wind turbines, such as barges, TLPs and semisubmersibles that are moderate or large in diameter or have complicated geometry.

## Mooring System Modelling

If a mooring system acts inherently linear and line inertia and damping are ignored, the total load on the support platform from the contribution of all mooring lines,  $F_i^{Lines}$ , from equation (4), is

$$F_i^{Lines} = F_i^{Lines,0} - C_{ij}^{Lines} q_j \quad (17)$$

where  $C_{ij}^{Lines}$  is the  $(i,j)$  component of the linearized restoring matrix from all mooring lines and  $F_i^{Lines,0}$  is the  $i$ th component of the total mooring system load acting on the support platform in its undisplaced position [as

included in equation (11)]. For catenary mooring lines,  $F_i^{Lines,0}$  represents the pre-tension at the fairleads from the weight of the cable not resting on the seafloor in water. If the catenary lines are neutrally buoyant,  $F_i^{Lines,0}$  is zero. For taut mooring lines,  $F_i^{Lines,0}$  is the result of pre-tension in the mooring lines from excess buoyancy in the tank when the support platform is undisplaced, including the contribution of the weight of the cable in water.  $C_{ij}^{Lines}$  is the combined result of the elastic stiffness of the mooring lines and the effective geometric stiffness brought about by the weight of the cables in water, depending on the layout of the mooring system.

In general, however, the response of a mooring system is not linear in nature; instead, nonlinearities are generally evident in the force-displacement relationships. To account for these nonlinearities, a quasi-static module was developed to model the nonlinear restoring loads from the mooring system of floating platforms, and this mooring system module has been interfaced to FAST and ADAMS.

This module can model an array of homogenous taut or slack catenary mooring lines. It accounts for the apparent weight in fluid, elastic stretching and seabed friction of each line, but neglects the individual line bending stiffness. But because the quasi-static module is fully coupled with FAST and ADAMS, it also accounts for the non-linear geometric restoration of the complete mooring system. By 'quasi-static', we mean that with the fairlead positions known for a given platform displacement at any instant in time, the mooring system module solves for the tensions within, and configuration of, each mooring line by assuming that each cable is in static equilibrium at that instant. Using the tensions and additional loading on the platform from hydrodynamics and loading on the RNA and tower from aerodynamics, FAST or ADAMS then solves the dynamic equations of motion for the accelerations of the rest of the system (platform, tower, and RNA). Next, FAST or ADAMS integrates in time to obtain new platform and fairlead positions at the next time step, repeating this process.

Clearly, this quasi-static approach also ignores the inertia and damping of the mooring system, which may or may not be important in various situations. To justify using this approach, the system-mass data presented in the Floating Platforms section below were used to calculate that the mass of a typical mooring system is 8% of the combined mass of a typical RNA, tower and floating support platform. From experience, about one-quarter of the inertia of a mooring system is important to the dynamic response of a floating platform. One-quarter of 8% is only 2%, which justifies ignoring mooring system inertia in the analyses for these floating wind turbine configurations. Ignoring mooring system damping is also a conservative approach.

Figure 4 presents a layout of the calculation procedures in the quasi-static mooring system module. Each line of the mooring system is analysed independently. The user must specify the fairlead locations of each mooring line relative (and fixed) to the support platform and the anchor locations of each mooring line relative (and fixed) to the inertial reference frame (i.e. the seabed). For each mooring line, the total unstretched length,  $L$ , apparent weight in fluid per unit length,  $w$ , extensional stiffness,  $EA$ , and coefficient of seabed static-friction drag,  $C_B$ , must also be assigned. Because a mooring line is buoyant,  $w$  is related to the mass of the line per unit length,  $\mu_c$ , by

$$w = \left( \mu_c - \rho \frac{\pi D_c^2}{4} \right) g \quad (18)$$

where  $\rho$  is the water density,  $g$  is the gravitational acceleration constant and  $D_c$  is the effective diameter of the mooring line.

Each mooring line is analysed in a local coordinate system that originates at the anchor. The local  $z$ -axis of this coordinate system is vertical and the local  $x$ -axis is directed horizontally from the anchor to the instantaneous position of the fairlead. Figure 5 illustrates a typical line. When the mooring system module is called for a given support platform displacement, the module first transforms each fairlead position from the global frame to this local system to determine its location relative to the anchor,  $x_F$  and  $z_F$ .

The analytical formulation for an elastic cable suspended between two points, hanging under its own weight (in fluid) was utilized. This analytical formulation was derived following a procedure similar to that presented in Faltinsen,<sup>24</sup> but extended to include seabed interaction and taut lines where the angle of the line at the anchor

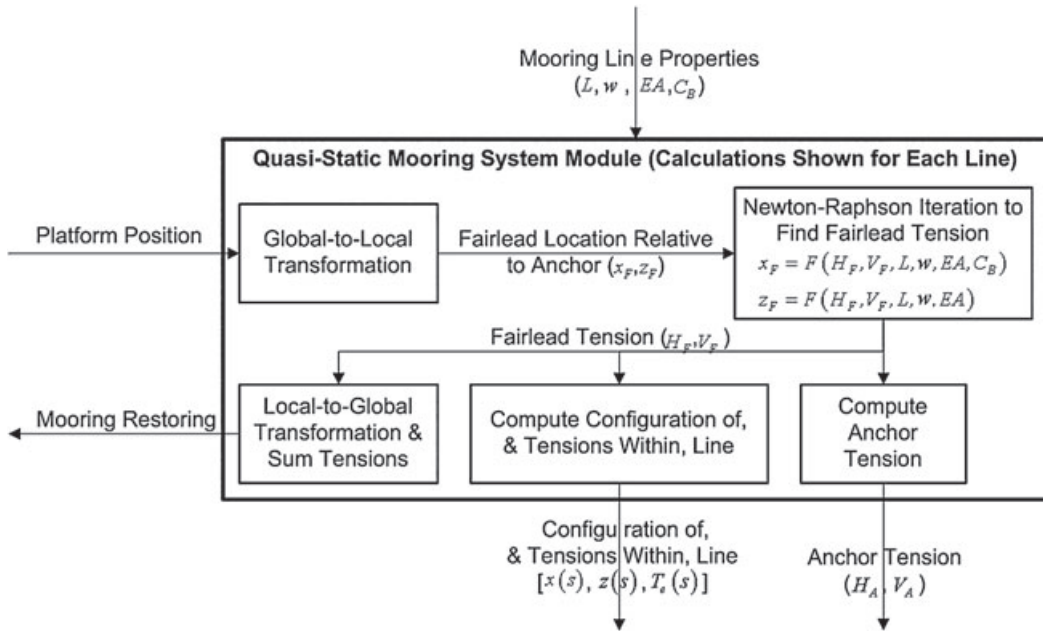


Figure 4. Summary of the mooring system module calculation procedure

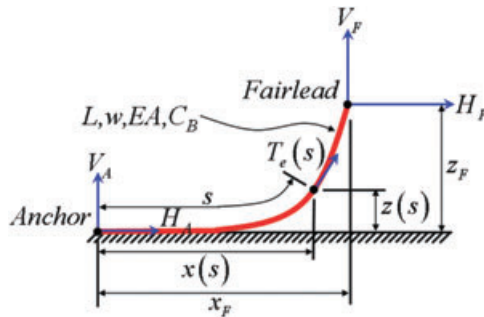


Figure 5. Mooring line in a local coordinate system

was non-zero. The derivation required the assumption that the extensional stiffness of the mooring line,  $EA$ , was much greater than the hydrostatic pressure at all locations along the line.

In the local coordinate system, the analytical formulation is given in terms of two nonlinear equations in two unknowns—the unknowns are the horizontal and vertical components of the effective tension in the mooring line at the fairlead,  $H_F$  and  $V_F$ , respectively. [The effective tension is defined as the actual cable (wall) tension plus the hydrostatic pressure.] When no portion of the line rests on the seabed, the analytical formulation is as follows:

$$x_F(H_F, V_F) = \frac{H_F}{w} \left\{ \ln \left[ \frac{V_F}{H_F} + \sqrt{1 + \left( \frac{V_F}{H_F} \right)^2} \right] - \ln \left[ \frac{V_F - wL}{H_F} + \sqrt{1 + \left( \frac{V_F - wL}{H_F} \right)^2} \right] \right\} + \frac{H_F L}{EA} \quad (19a)$$

and

$$z_F(H_F, V_F) = \frac{H_F}{w} \left[ \sqrt{1 + \left( \frac{V_F}{H_F} \right)^2} - \sqrt{1 + \left( \frac{V_F - wL}{H_F} \right)^2} \right] + \frac{1}{EA} \left( V_F L - \frac{wL^2}{2} \right) \quad (19b)$$

The first terms on the right-hand side of equation (19) characterize the arc length of the catenary, projected on the  $x$ - and  $z$ -axes (even taut mooring lines have a catenary-shaped sag). The second terms on the right-hand side of equation (19) represent the horizontal and vertical stretching of the mooring line.

The analytical formulation of two equations in two unknowns is different when a portion of the mooring line adjacent to the anchor rests on the seabed:

$$x_F(H_F, V_F) = L - \frac{V_F}{w} + \frac{H_F}{w} \ln \left[ \frac{V_F}{H_F} + \sqrt{1 + \left( \frac{V_F}{H_F} \right)^2} \right] + \frac{H_F L}{EA} + \frac{C_B w}{2EA} \left[ - \left( L - \frac{V_F}{w} \right)^2 + \left( L - \frac{V_F}{w} - \frac{H_F}{C_B w} \right) \text{MAX} \left( L - \frac{V_F}{w} - \frac{H_F}{C_B w}, 0 \right) \right] \quad (20a)$$

and

$$z_F(H_F, V_F) = \frac{H_F}{w} \left[ \sqrt{1 + \left( \frac{V_F}{H_F} \right)^2} - \sqrt{1 + \left( \frac{V_F - wL}{H_F} \right)^2} \right] + \frac{1}{EA} \left( V_F L - \frac{wL^2}{2} \right) \quad (20b)$$

The first two terms on the right-hand side of equation (20a) combine to represent the unstretched portion of the mooring line resting on the seabed,  $L_B$ :

$$L_B = L - \frac{V_F}{w} \quad (21)$$

In equation (19),  $L_B$  is zero.

The last term on the right-hand side of equation (20a), which involves  $C_B$ , corresponds to the stretched portion of the mooring line resting on the seabed that is affected by static friction. The seabed static friction was modelled simply as a drag force per unit length of  $C_B w$ . The *MAX* function is needed to handle cases with and without tension at the anchor. Specifically, the resultant is zero when the anchor tension is positive; that is, the seabed friction is too weak to overcome the horizontal tension in the mooring line. Conversely, the resultant of the *MAX* function is nonzero when the anchor tension is zero. This happens when a section of cable lying on the seabed is long enough to ensure that the seabed friction entirely overcomes the horizontal tension in the mooring line.

The remaining terms in equation (20) are similar in form to, and typify the same information as, the terms in equation (19). They are simpler than the terms in equation (19), however, because a slack catenary is always tangent to the seabed at the point of touchdown.

The mooring system module uses a Newton–Raphson iteration scheme to solve non-linear equations (19) and (20) for the fairlead effective tension ( $H_F$  and  $V_F$ ), given the line properties ( $L$ ,  $w$ ,  $EA$  and  $C_B$ ) and the fairlead position relative to the anchor ( $x_F$  and  $z_F$ ). The Jacobian in the Newton–Raphson iteration was implemented with the analytical partial derivatives of equation (19) and (20). The mooring system module determines which of equation (19) or (20) must be used as part of the solution process. The equations were implemented in a slightly different form than shown to avoid numerical problems (e.g. a division by zero when  $C_B$  is zero-valued). The module uses the values of  $H_F$  and  $V_F$  from the previous time step as the initial guess in the next iteration of Newton–Raphson. Jonkman<sup>16</sup> describes how the module is initialized.

Once the effective tension at the fairlead has been found, determining the horizontal and vertical components of the effective tension in the mooring line at the anchor,  $H_A$  and  $V_A$ , respectively, is simple (the arrows depicting  $H_A$  and  $V_A$  in Figure 5 are the horizontal and vertical components of the effective line tension at the anchor—they are not the reaction forces at the anchor). From a balance of external forces on a mooring line, one can easily verify that

$$H_A = H_F \quad (22a)$$

and

$$V_A = V_F - wL \quad (22b)$$

when no portion of the line rests on the seabed, and

$$H_A = \text{MAX}(H_F - C_B w L_B, 0) \quad (23a)$$

and

$$V_A = 0 \quad (23b)$$

when a portion of the line does rest on the seabed. Although they do not affect the dynamic response of the floating wind turbine system, the anchor effective tensions are computed by the mooring system module and become available outputs from the simulation.

Next, the mooring system module solves for the configuration of, and effective tensions within, the mooring line. Again, the values of these parameters do not affect the dynamic response of the floating wind turbine system, but they are available outputs from the simulation. Jonkman<sup>16</sup> describes how these parameters are formulated.

As shown in Figure 4, the last calculation in the quasi-static mooring system module is a computation of the total load on the support from the contribution of all mooring lines; that is,  $F_i^{Lines}$  from equation (4). This mooring system-restoring load is found by first transforming each fairlead tension from its local mooring line coordinate system to the global frame, then summing up the tensions from all lines.

### **Merging the Aero-hydro-servo-elastic Capabilities**

The developed simulation tools are capable of modelling the fully coupled aero-hydro-servo-elastic response of offshore floating wind turbines by leveraging the computational methodologies and analysis tools of the land-based wind turbine and offshore O&G industries. The land-based wind-industry-accepted aero-servo-elastic turbine simulation capabilities of FAST<sup>17</sup> with AeroDyn<sup>18</sup> and MSC.ADAMS with A2AD<sup>19</sup> and AeroDyn have been interfaced with the external hydrodynamic wave-body interaction program WAMIT,<sup>20</sup> which is commonly used in the offshore O&G industry. The interfaces among these simulation capabilities were established by developing modules for treating time-domain hydrodynamics (HydroDyn) and quasi-static mooring system responses.

Turbulent-wind inflow is prescribed by the external computer program TurbSim.<sup>32</sup> FAST with AeroDyn and ADAMS with AeroDyn account for the applied aerodynamic and gravitational loads, the behaviour of the control and protection systems, and the structural dynamics of the wind turbine. The latter contribution includes the elasticity of the RNA and tower, along with the newly added dynamic coupling between their motions and the motions of the support platform. Non-linear restoring loads from the mooring system are obtained from a quasi-static mooring line module that accounts for the elastic stretching of an array of homogenous taut or slack catenary lines with seabed interaction. The HydroDyn hydrodynamics module accounts for linear hydrostatic restoring; nonlinear viscous drag from incident-wave kinematics, sea currents and platform motion; the added-mass and damping contributions from linear wave radiation, including free-surface memory effects; and the incident-wave excitation from linear diffraction in regular or irregular seas. Aerodynamic loads depend on the shape of the rotor-blade airfoils; in a similar way, hydrodynamic loads depend on the support platform's geometry. To this end, HydroDyn has been developed such that the hydrodynamic coefficients for platforms of arbitrary shape are imported from WAMIT or an equivalent hydrodynamic pre-processor.

By interfacing these modules as described, fully coupled time-domain aero-hydro-servo-elastic simulation of offshore floating wind turbines is achieved. This capability is crucial for analyzing the dynamic response from combined wind and wave loading because both can affect the motions, loads, and power production of the system. The generality of each module also ensures that the overall simulation tool is universal enough to analyze a variety of RNA, tower, support platform and mooring system configurations. Moreover, the same

simulation tools can still be used to model land-based wind turbines by disabling the hydrodynamic and mooring system modules.

### ***Wind Turbine and Floating Platform Model Descriptions***

To support concept studies aimed at assessing offshore wind technology, use of realistic and standardized input data is required. NREL developed the specifications of a representative utility-scale multi-megawatt turbine now known as the ‘NREL offshore 5-MW baseline wind turbine’. The two floating support platforms used in this work were developed by others through partnerships with NREL. Both platforms are barge concepts developed specifically to support the RNA and tower of the NREL offshore 5 MW system. Barge concepts were chosen because of their simplicity in design, fabrication, and installation.

#### ***NREL Offshore 5 MW Baseline Wind Turbine***

The NREL offshore 5 MW baseline wind turbine is a conventional three-bladed upwind variable-speed variable blade-pitch-to-feather-controlled turbine. To create the model, some broad design information from the published documents of turbine manufacturers, with a heavy emphasis on the REpower 5M machine, was obtained. Because detailed data was unavailable, however, publicly available properties of conceptual models from several projects were also used. A composite was then created from these data, extracting the best available and most representative specifications. The specifications consist of definitions of the aerodynamic, structural and control-system properties. Table I summarizes some of these properties. Greater detail is available in Jonkman *et al.*<sup>33</sup>

#### ***Floating Platforms***

For some of the simulation code verification exercises, the RNA and tower of the NREL 5 MW baseline system were modelled mounted on a floating barge from ITI Energy. A preliminary barge concept developed from the Department of Naval Architecture and Marine Engineering (NAME) at the Universities of Glasgow and Strathclyde through a contract with ITI Energy was used. Not only is the barge intended to support the 5 MW RNA and tower, but it is also a platform for an oscillating water column wave-power device. To ensure that the simplest possible manufacturing techniques can be used in its fabrication, the barge is square and the wave energy is extracted from a square moon pool located at the centre of the barge, which allows the oscillating water column to be installed within the tower. The barge is ballasted with seawater to achieve a reasonable draft, which is not so shallow that it is susceptible to incessant wave slamming. To prevent it from drifting,

Table I. Summary of properties for the NREL 5 MW baseline wind turbine

Rating	5 MW
Rotor orientation, configuration	Upwind, three blades
Control	Variable speed, collective pitch
Drivetrain	High speed, multiple-stage gearbox
Rotor, hub diameter (m)	126, 3
Hub height (m)	90
Cut-in, rated, cut-out wind speed ( $M s^{-1}$ )	3, 11.4, 25
Cut-in, rated rotor speed (rpm)	6.9, 12.1
Rated tip speed ( $m s^{-1}$ )	80
Overhang, shaft tilt, pre-cone	5 m, 5°, 2.5°
Rotor mass (kg)	110,000
Nacelle mass (kg)	240,000
Tower mass (kg)	347,500
Coordinate location of overall CM (m)	-0.2, 0.0, 64.0

the platform is moored by a system of eight slack catenary lines. Two of these lines emanate from each corner of the bottom of the barge such that they would be 45° apart at the corner. Some details of the ITI Energy barge and mooring system are provided in Table II. The concept is documented in much greater detail in Vijfhuizen.<sup>7</sup>

Note, however, that some of the properties given in Table II disagree with the data published in Vijfhuizen<sup>7</sup> because an updated design has been used. The published freeboard of 4 m in Vijfhuizen<sup>7</sup> was increased to 6 m after wave tank testing at NAME demonstrated that more freeboard would be beneficial to the system's response. This changed the CM location and inertias slightly. In addition, Vijfhuizen<sup>7</sup> used a simple linearized representation of the mooring system. The more detailed mooring system documented in Table II was developed after Vijfhuizen<sup>7</sup> was published. Also note that the capabilities of the aero-hydro-servo-elastic simulation tools do not permit an oscillating water column wave-power device or its associated potential for energy extraction to be modelled. Instead, the hydrodynamics of the barge were modelled by assuming that the moon pool was covered by a fixed plate located just below the free surface. The WAMIT Output/HydroDyn Input section below explains this assumption in more detail.

MIT also developed preliminary concepts of several floating platforms for the RNA and tower of the NREL offshore 5 MW baseline system. One of the designs is named the MIT/NREL shallow-drafted barge (herein, MIT/NREL barge). The RNA and tower of the 5 MW baseline system were also mounted on this floating platform for some of the simulation code verification exercises. The MIT/NREL barge is a cylindrical barge and has a spread-mooring system with four pairs of taut lines that radiate outward. Some of the barge data is listed in Table III; the concept is documented in much greater detail in Wayman.<sup>6</sup>

## Overview of the Simulation Verification

The aero-servo-elastic capabilities of FAST with AeroDyn and ADAMS with AeroDyn have been well verified and validated in previous studies.<sup>34–36</sup> But because the hydrodynamics and mooring system modules are novel, they must be verified to ensure that the response predictions from the fully coupled aero-hydro-servo-elastic capability are accurate. In all, seven verification studies were performed to test the accuracy of the new features: three for the hydrodynamics module, two for the mooring system module and two for the complete system. The last pair of verification exercises compared the results from the time-domain simulation tool with the results from a frequency-domain model. Additionally, though not explicitly documented here, the resulting dynamics from the newly added support platform DOFs in FAST agree well with ADAMS. Model-to-model

Table II. Summary of ITI Energy barge properties

Size (W × L × H) (m)	40 × 40 × 10
Moon pool (W × L × H) (m)	10 × 10 × 10
Draft, freeboard (m)	4, 6
Water displacement (m <sup>3</sup> )	6,000
Mass, including ballast (kg)	5,452,000
CM location below SWL (m)	0.2818
Roll inertia about CM (kg m <sup>2</sup> )	726,900,000
Pitch inertia about CM	726,900,000
Yaw inertia about CM	1,454,000,000
Anchor (water) depth (m)	150
Separation between opposing anchors (m)	773.8
Unstretched line length (m)	473.3
Neutral line length resting on seabed (m)	250
Line diameter (m)	0.0809
Line mass density (kg m)	130.4
Line extensional stiffness (N)	589,000,000

Table III. Summary of MIT/NREL barge properties

Diameter, height (m)	36 m, 9.5
Draft, freeboard (m)	5 m, 4.5
Water displacement (m <sup>3</sup> )	5,089
Mass, including ballast (kg)	4,519,000
CM location below SWL (m)	3.882
Roll inertia about CM (kg m <sup>2</sup> )	390,100,000
Pitch inertia about CM (kg m <sup>2</sup> )	390,100,000
Yaw inertia about CM (kg m <sup>2</sup> )	750,900,000
Anchor (water) depth (m)	200
Separation between opposing anchors (m)	436
Unstretched line length (m)	279.3
Neutral line length resting on seabed (m)	0
Line diameter (m)	0.127
Line mass density (kg m)	116.0
Line extensional stiffness (N)	1,500,000,000
Diameter, height (m)	36 m, 9.5

comparisons were used for all these verification exercises. The fully coupled simulation tool will be validated later, once experimental data are made available.

### Verification of the Hydrodynamics Module

Three verification tests were performed to check HydroDyn's hydrodynamics calculations. The first test verified that the PSD of the wave-elevation time series computed by HydroDyn matched the target JONSWAP spectrum prescribed by HydroDyn's wave-spectrum input parameters. The second test verified that the output from WAMIT, which is used as input to HydroDyn, is similar to that generated by a different radiation/diffraction solver. The third test verified that the radiation impulse-response functions computed within the hydrodynamics module were the same as those computed with WAMIT's stand-alone frequency-to-time (F2T) conversion utility.<sup>20</sup>

### Wave Elevation versus the Target Wave Spectrum

Irregular sea states (stochastic waves) are modelled in HydroDyn by the inverse Fourier transform of equation (6), which represents the superposition of a large number of periodic and parallel wave components. The amplitudes of these wave components, on average, are determined by the prescribed wave spectrum.

A simple test was run to check that these mathematical relationships were implemented correctly in HydroDyn. Four wave-elevation time series were computed, each determined with the Pierson–Moskowitz wave spectrum given by a significant wave height,  $H_s$ , of 5.49 m and a peak spectral period,  $T_p$ , of 14.66 s or a peak spectral frequency of about 0.429 rad s<sup>-1</sup> [this spectrum is equivalent to a JONSWAP spectrum with the default value (unity) of the peak shape parameter]. Each wave-elevation time series was 10,000 s long (i.e. just short of 3 h each) and was differentiated through the choice of dissimilar random seeds.

The PSD of each wave-elevation record was then computed and compared to the target wave spectrum determined by the given spectral parameters. Figure 6 shows the results. To minimize scatter, the discrete-frequency PSD data of Figure 6 are grouped in bins of width 0.001 Hz (about 0.00628 rad s<sup>-1</sup>). Because of the normally distributed amplitudes provided by the white Gaussian noise process, however, there is still a fair amount of scatter in the PSD of each individual run. But the average of the four PSDs, as indicated by the series labelled 'Run Average' in Figure 6, is approaching the target spectrum nicely. This outcome would improve by averaging the results of many more simulations or by disabling the normally-distributed amplitudes.

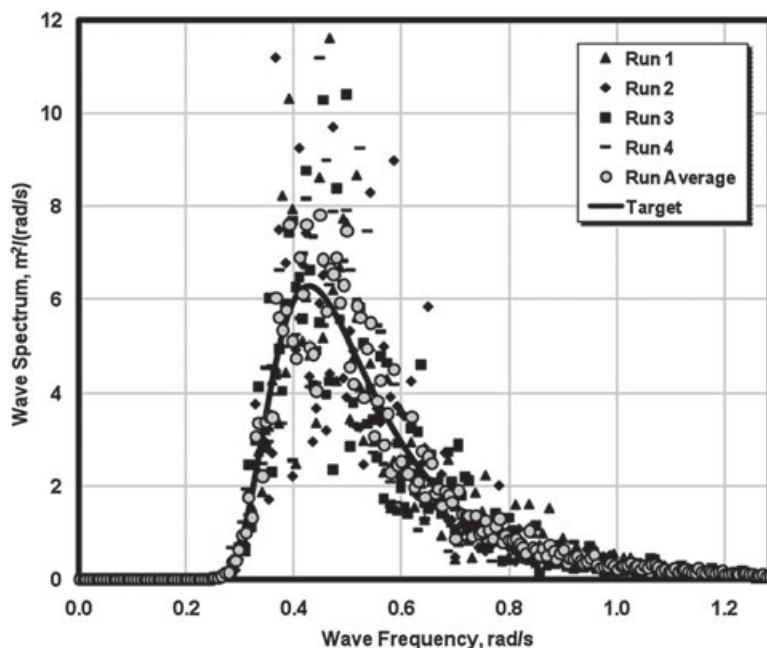


Figure 6. PSD of wave elevations versus target wave spectrum

The probability density was also calculated for the aggregate composite of the wave-elevation records computed by, and output from, HydroDyn. The results are not shown here, but as expected, this histogram is Gaussian-distributed with a mean of zero and a standard deviation (SD) (for this test case) of  $H_s/4 = 1.37$  m.

### WAMIT Output/HydroDyn Input

WAMIT<sup>20</sup> is used as a pre-processor for generating the hydrodynamic-added-mass and -damping matrices,  $A_{ij}(\omega)$  and  $B_{ij}(\omega)$ , and wave-excitation force,  $X_i(\omega, \beta)$ , which are inputs to HydroDyn. WAMIT uses the three-dimensional numerical-panel method to solve the linearized hydrodynamic radiation and diffraction problems for the interaction of surface waves with offshore platforms in the frequency domain. WAMIT ignores the effects of sea current or forward speed on the radiation and diffraction problems, as well as higher-order effects.

Because the hydrodynamic solution the simulation tool generates is only as good as the hydrodynamic inputs, verifying the acceptability of the WAMIT results is beneficial. Consequently, a test was run to ensure that the generated WAMIT output is similar to that calculated by a different radiation/diffraction solver. Data used by NAME at the Universities of Glasgow and Strathclyde when devising the ITI Energy barge were available for this comparison. NAME used a custom-made linear hydrodynamic radiation and diffraction solver with capabilities similar to, but independent of, WAMIT.

The barge was modelled in WAMIT with two geometric planes of symmetry with 2,400 rectangular panels within a quarter of the body. Consistent with linear theory, only the wetted portion of the body in its undisplaced position needed to be meshed. To avoid accounting for the oscillating water column in the WAMIT analysis, the moon pool was covered with a fixed plate located 0.01 m below the free surface.

The barge was analysed in its undisplaced position with infinite water depth in both codes. The hydrodynamic-added-mass and -damping matrices were compared in all six rigid-body modes of motion of the barge (in the matrix subscripts, 1 = surge, 2 = sway, 3 = heave, 4 = roll, 5 = pitch, 6 = yaw), resulting in  $6 \times 6$  matrices at each frequency. The hydrodynamic wave-excitation force was not considered in this test. Figure 7 shows the results in a side-by-side comparison. All data are dimensional as indicated. Only the upper

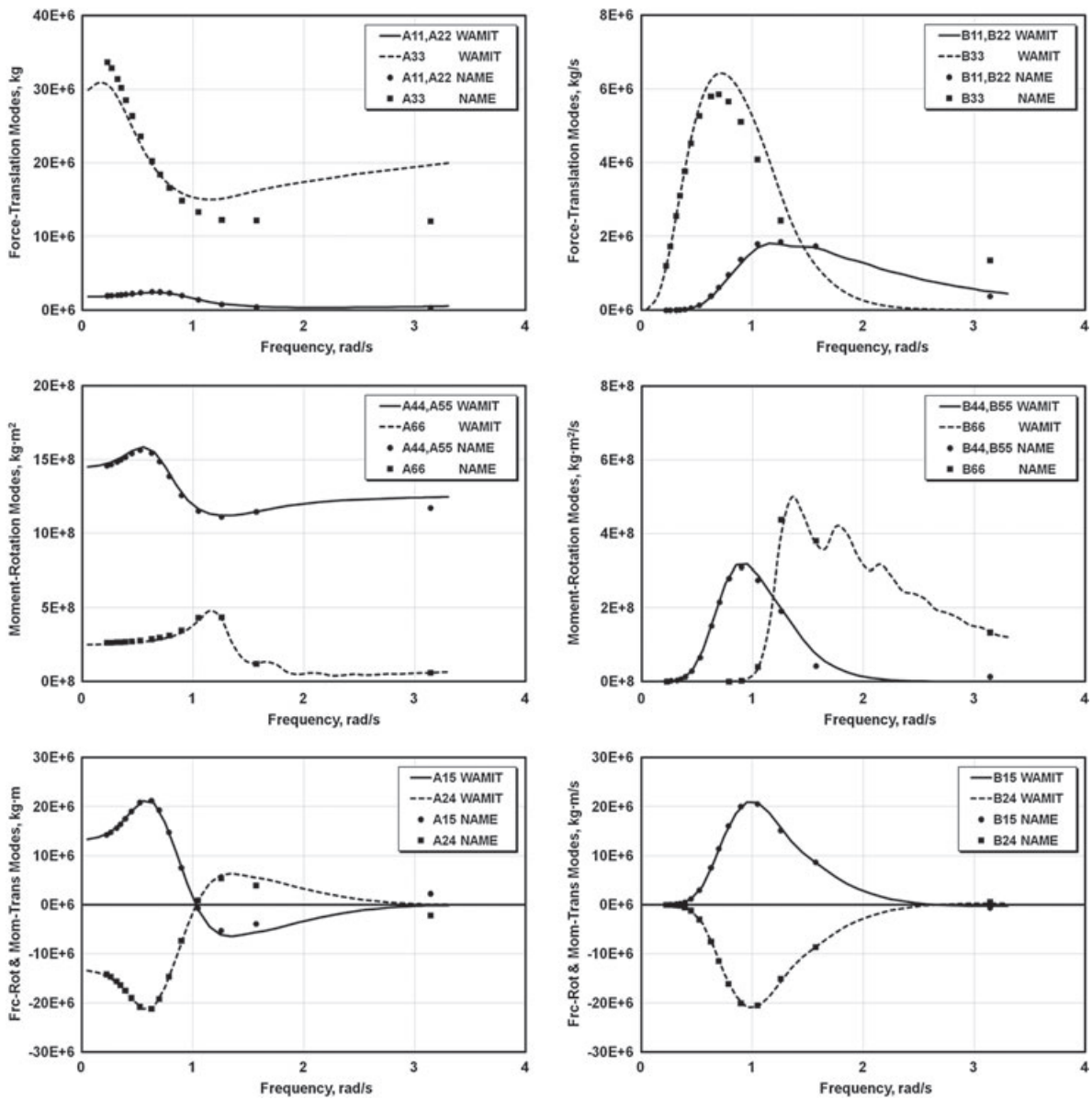


Figure 7. Hydrodynamic added mass and damping for the ITI Energy barge

triangular matrix elements are shown because the hydrodynamic-added-mass and -damping matrices are symmetric in the absence of sea current or forward speed.<sup>24,25</sup> Also, because of the barge’s symmetries, the surge-surge elements of the frequency-dependent added-mass and damping matrices,  $A_{11}$  and  $B_{11}$ , are identical to the sway-sway elements,  $A_{22}$  and  $B_{22}$ . Similarly, the roll-roll elements,  $A_{44}$  and  $B_{44}$ , are identical to the pitch-pitch elements,  $A_{55}$  and  $B_{55}$ . Other matrix elements not shown are zero-valued or very close to being zero-valued.

In Figure 7, the WAMIT results are given in even increments of frequency. The NAME results are given in even increments of period, so resolution is lost at the higher frequencies. As expected, all matrix elements peak out at some intermediate frequency and level out at higher frequencies. Additionally, the zero- and

infinite-frequency limits of all elements of the hydrodynamic-damping matrix are zero (not all shown), as required by theory.<sup>24,25</sup> The comparisons between the output of WAMIT and the results of NAME generally agree very well and demonstrate that WAMIT is an acceptable code for generating the hydrodynamic inputs needed by the simulation tool. The biggest discrepancies are in the heave–heave elements of the frequency-dependent added-mass and damping matrices,  $A_{33}$  and  $B_{33}$ . These differences are probably artefacts of the dissimilar numerical solutions employed by WAMIT and NAME's radiation/diffraction solver. The differences are not large, however, and are not believed to be crucial to the accuracy of the hydrodynamics solution.

### *Computation of Radiation Impulse-Response Functions*

The radiation 'memory effect' is captured in HydroDyn's hydrodynamics module through the convolution integral of equation (5). As described earlier, the kernel,  $K_{ij}(t)$ , in this convolution integral is commonly referred to as the impulse-response functions of the radiation problem and can be found from the solution of the frequency-domain radiation problem. In HydroDyn specifically, these functions are found using the cosine transform of the frequency-dependent hydrodynamic-damping matrix, as given in equation (15b). As in the verification of the wave-elevation computation, it was important to verify that this cosine transform was implemented correctly.

This verification was performed by testing that the radiation impulse-response functions computed within HydroDyn are the same as those computed by WAMIT's stand-alone F2T conversion utility. The cosine transform was implemented within HydroDyn, as opposed to having HydroDyn read in the output of WAMIT's F2T utility, because many of the other computer codes available to solve the frequency-domain hydrodynamics problem do not contain the F2T conversion functionality. This test used the WAMIT output of the frequency-dependent hydrodynamic-damping matrix for the ITI Energy barge from the previously presented verification test.

Because the comparison between the F2T and HydroDyn results is so good (i.e. the results are essentially identical), only one set of results is presented in Figure 8. As before, all data are dimensional as indicated, and because of the symmetries of the barge, the surge–surge elements are identical to the sway–sway elements, and the roll–roll elements are identical to the pitch–pitch elements. Most of the response decays to zero after about 20 s (as shown) and has all but vanished at 60 s (not shown). Consequently, to speed up the calculations of the memory effect in the simulation tool, the numerical convolution is generally truncated after 60 s of memory.

### **Verification of the Mooring System Module**

Two verification tests were performed to check the quasi-static mooring system module. The first test verified that the mooring system module correctly solves a classic benchmark problem for the static equilibrium of a suspended-cable mechanism. The second test verified that the nonlinear force-displacement relationships for a mooring system in surge, as computed by the module, were the same as those calculated by an independent analysis performed by NAME.

#### *Benchmark Problem*

A classic test problem<sup>37</sup> for checking the accuracy of a mooring system program is that of a horizontally suspended cable with one support free to slide laterally. Figure 9 illustrates this problem. For a cable of an unstretched length of  $L = 200$  m, a weight per unit length of  $w = 0.1$  N m<sup>-1</sup>, an extensional stiffness of  $EA = 10^5$  N and a horizontal load (equivalent to the horizontal tension at the fairlead) of  $H_F = 5.77$  N applied at the free end (the fairlead), the theoretical static-equilibrium solution is for a horizontal span of  $x_F = 152.2$  m and a vertical sag of 58.0 m.

Because FAST and ADAMS both operate in the time domain, the mooring system module was tested by solving this problem through time integration of the non-linear equations of motion. The platform, where the

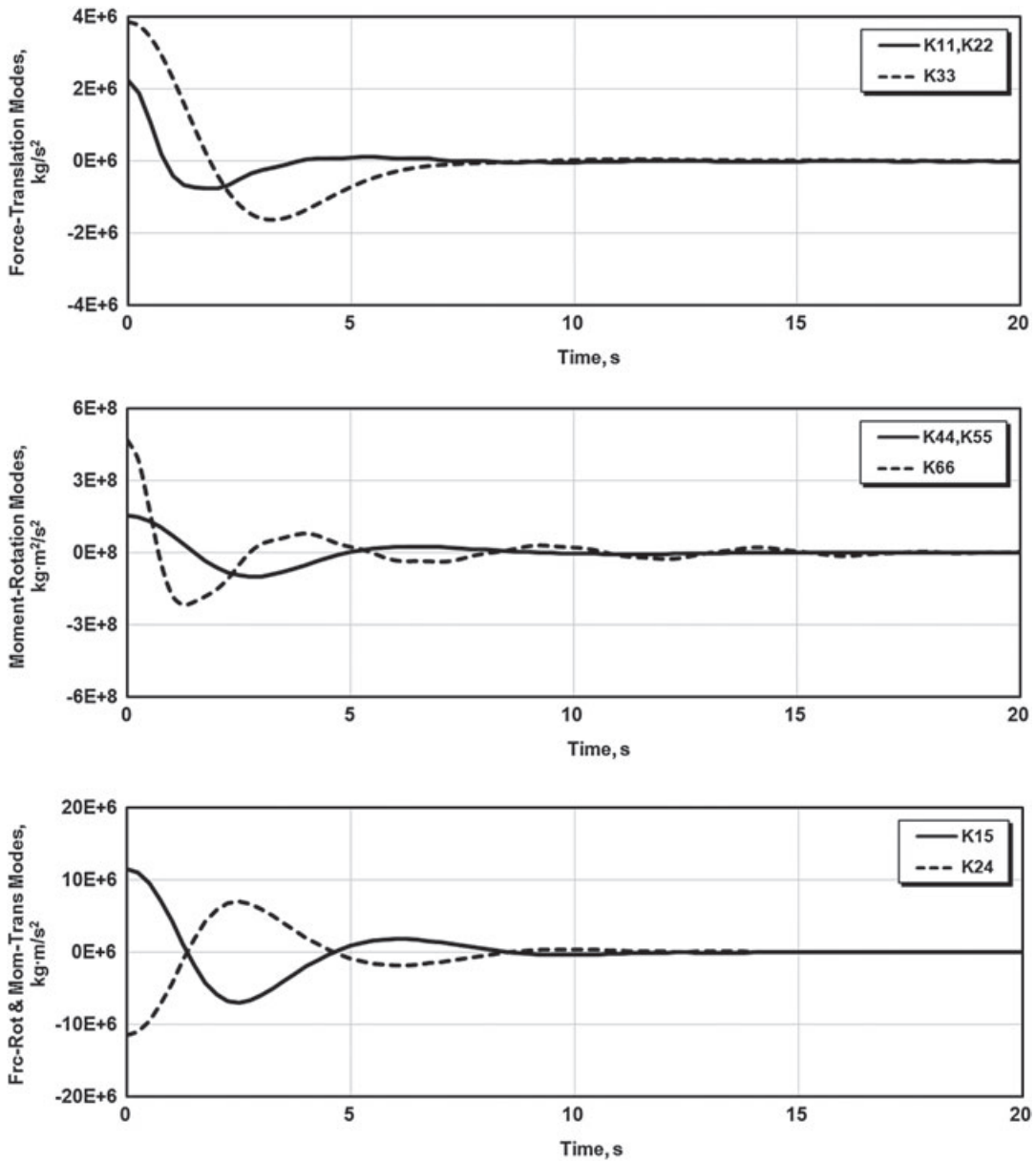


Figure 8. Radiation impulse-response functions for the ITI Energy barge

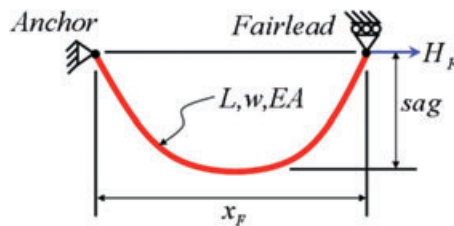


Figure 9. Benchmark problem for a suspended cable

fairlead attaches, was given one horizontal-translation DOF, a small inconsequential mass and a small amount of linear damping so as to ensure that the motion eventually settled out. The horizontal span and vertical sag converged to the correct solution (not shown) regardless of the lateral offset chosen as an initial condition for the DOF.

### Non-linear Force-displacement Relationships

Non-linearities are evident in the force-displacement relationships of most mooring systems. Because these non-linearities may be important in the dynamic response of offshore floating wind turbines, the quasi-static mooring system module must be checked to ensure it is computing them correctly.

NAME used a custom-made mooring analysis program to develop the mooring system for the ITI Energy barge. NAME's program accounts for homogenous taut or catenary lines with horizontal (but not vertical) elastic stretching. A portion of a line may rest on the seabed in NAME's mooring program, but the program does not account for seabed friction. Even though NAME's program has fewer capabilities than the developed mooring system module, the analysis module was verified by comparing its response with NAME's.

As discussed earlier, the layout of the mooring system for the ITI Energy barge consists of eight catenary lines. In this verification test, however, the layout was modified to make the mooring lines parallel to the sides of the barge because this is the only way NAME's program could model it. With this modification, each pair of lines is 90° apart at the corner and opposing lines are parallel to each other. NAME computed the force-displacement relationships for surge motions of the barge for each line independently as well as opposing lines jointly. To reproduce NAME's results, a model of the barge and mooring system was built with the mooring system module interfaced to ADAMS, and the barge was translated in surge through a time-marching simulation. This time-dependent motion of the barge does not affect the results of the analysis because the mooring lines are treated quasi-statically in the module.

As in previous verification tests, the results from this exercise compared very well. Because the agreement is so good (i.e. the results are essentially identical), again, only the quasi-static mooring system module results are presented, as shown in Figure 10. There is a horizontal tension of about 100 kN in each line when the barge is in its neutral position. The force-displacement curve for opposing lines, which represents the net horizontal restraining force on the barge, remains fairly linear between +20 m and -20 m of surge motion. Beyond a surge displacement of about 40 m, the resistance of the mooring system increases dramatically because the upwind line gets much tauter (likewise for the downwind line beyond -40 m of surge displacement). At 50 m of surge displacement, the horizontal tension in the upwind line exceeds 1,000 kN (likewise for the downwind line at -50 m of surge displacement).

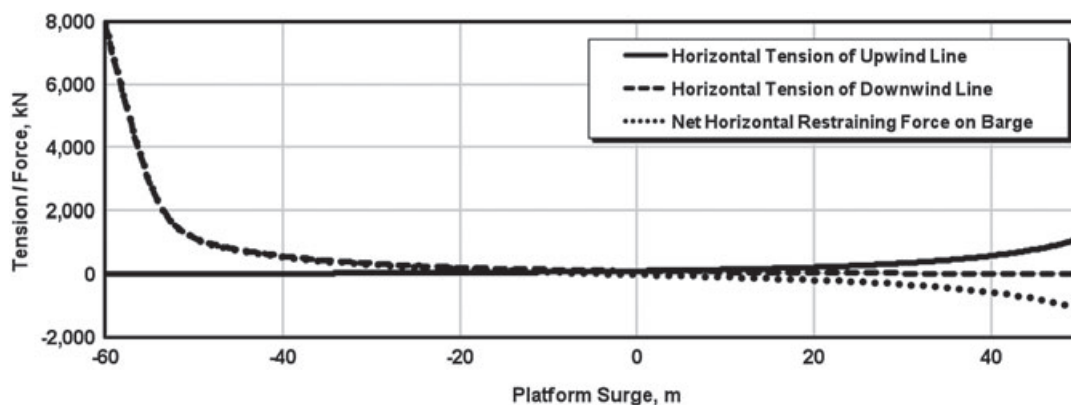


Figure 10. Force-displacement relationships for the ITI Energy mooring system

## ***Time Domain versus Frequency Domain Verification***

Because the fully coupled aero-hydro-servo-elastic simulation tool is the first of its kind to be developed, finding independent model results to use for verification is difficult. The time-domain models that others have previously developed and used to analyze offshore floating wind turbines were either not rigorous enough to yield sufficient verification data or were unavailable for use.<sup>8–15</sup> Many of the previous studies related to offshore floating wind turbines used frequency-domain models.<sup>4–7</sup> The results of a frequency-domain analysis can be used to verify the simulation tool because the hydrodynamic theory in the module was derived from the time-domain representation of the frequency-domain problem. Two such verifications are presented here.

Frequency-domain solutions describe the sinusoidal steady-state response of a platform to incident waves that propagate at a single amplitude, frequency and direction. The solution to the frequency-domain problem is generally given in terms of response amplitude operators (RAOs), which are the complex-valued amplitudes of motions for each DOF of the support platform, normalized per unit of wave amplitude. Imaginary components indicate that the response is out of phase with the wave elevation. In a time-domain model, the sinusoidal steady-state response of a floating platform can be found by introducing regular, periodic waves as forcing functions, and simulating in time long enough to ensure all transient behaviour has died out. As a first verification of the fully coupled model, such time-series simulations were utilized to back out the RAOs at discrete incident-wave frequencies, and the process was repeated to find the RAOs at each desired frequency. For this verification test, Wayman's frequency-domain results were used for the MIT/NREL barge (see Wayman<sup>6</sup>).

The response of a floating platform to stochastic sea states in the frequency-domain problem can only be characterized statistically because the frequency-domain representation is not valid for transient analysis. Specifically, the motion of a linearized floating body will have a response that is Gaussian-distributed when it is excited by a sea state with a Gaussian-distributed wave elevation. The SDs of the motion response are dictated by the Wiener–Khinchine theorem.<sup>6</sup> In a time-domain model, the distributions of the motion response can be ascertained by post-processing the output of a series of simulations that are long enough to ensure that the results are statistically reliable (the process can be repeated to find the distributions at each desired sea state). This procedure was used as a second verification of the fully coupled, time-domain model, again using Wayman's<sup>6</sup> frequency-domain results for the MIT/NREL barge for comparison.

Wayman used WAMIT to compute the frequency-domain hydrodynamic properties of the MIT/NREL barge and modelled the spread-mooring system with linear restoring of  $4,000 \text{ kN m}^{-1}$  only in the surge and sway DOFs. The attributes of the RNA and tower were included in Wayman's linearized system model by augmenting the body-mass matrix with the mass properties of the RNA and tower and by augmenting the hydrodynamic-damping and -restoring matrices with damping and restoring contributions from rotor aerodynamics and gyroscopics. Wayman ignored the elasticity of the RNA and tower and considered only the six rigid-body modes of the barge.<sup>6</sup>

### ***Verification with Steady-state Response***

For this comparison, a FAST with AeroDyn and HydroDyn model of the RNA and tower of the NREL offshore 5 MW baseline system installed on the MIT/NREL barge was constructed. To ensure reasonable similarity to Wayman's model and to isolate the behaviour of the hydrodynamics and mooring system, the floating wind turbine was modelled without any control system (i.e. using constant rotor speed and fixed blade pitch) or any modes of motion other than the six rigid-body DOFs of the floating support platform. For environmental conditions, a constant unsheared  $11.2 \text{ m s}^{-1}$  wind (as Wayman used) and regular periodic waves of unit amplitude (a peak-to-peak height of 2 m) were used. Both the wind and waves were co-directional and aligned with the surge coordinate.

In the first attempt to run the time-domain simulations, the spread-mooring system was modelled with the quasi-static mooring system module interfaced to FAST. It was soon discovered, however, that the non-linear restoring of the spread-mooring system prohibited the response from ever reaching a sinusoidal steady-state condition, which eliminated any possibility of backing out the RAOs. To get around this, the interface to the mooring module was removed, and instead, the mooring system was modelled with linear restoring (in surge

and sway only) like in Wayman's model. As a consequence, the results presented next are not useful for verifying the time-domain implementation of the mooring system module. They are, however, still useful for verifying the time-domain implementation of the hydrodynamics module.

With the linearized mooring system model, a series of simulations were run, each 2,000 s in length to give them time to reach a periodic steady state. Even after all that time, the platform motion was still not perfectly sinusoidal for the sway, roll and yaw responses. Ten simulations were run with the discrete frequency of the incident waves varying from 0.15 to 1.05 rad s<sup>-1</sup> in even increments. Using the last cycle from each simulation, the amplitudes of the oscillations were computed for the three translational and three rotational platform responses. Because the incident waves were unit amplitude, these response amplitudes are equivalent to the magnitudes of the RAOs. For the rotational responses, the RAOs were normalized by the platform radius (18 m), as in Wayman's study.<sup>6</sup> These results are added to the non-dimensional RAO plots that Wayman had generated. In these tests, the phases of the response were not compared.

As shown in Figure 11, the time-domain predictions closely mimic those from Wayman's frequency-domain analysis for the platform-surge and -heave modes. This gave confidence that the time-domain implementation of the platform hydrodynamics was correct. The platform-pitch curves seem to have a similar character, but portions differ in both magnitude and frequency. The other three parameters—sway, roll and yaw—have such small responses that comparison is difficult. Because the oscillations of these modes had not become completely sinusoidal after 2,000 s, we question whether those comparisons are meaningful. Even though there is no excitation of the platform-yaw mode from aerodynamics or hydrodynamics in this configuration, the yaw response is non-zero because the spinning inertia of the rotor, combined with the pitching motion of the platform, induces a gyroscopic yaw moment.

The differences in the pitch RAO are believed to be caused by the variation between the two models for the aerodynamic damping in pitch. Wayman showed that the platform damping in pitch is completely dominated by rotor aerodynamics, not by wave radiation (see Appendix A.1 of Wayman<sup>6</sup>). This is not true for the other modes of motion, such as surge and heave. In Wayman's analysis, the aerodynamic damping in barge pitch was constant (it was derived using FAST with AeroDyn to linearize the rotor aerodynamic thrust about the mean pitch orientation of the platform). In contrast, the aerodynamic damping in barge pitch in our model varies as the rotor oscillates against and with the wind.

### *Verification with Stochastic Response*

To verify the stochastic response, three FAST with AeroDyn and HydroDyn models of the RNA and tower of the NREL offshore 5 MW baseline system installed on the MIT/NREL barge were built. The first was the same one used in the RAO comparison: it had a rigid RNA and tower, no control system, and a linearized form of the mooring system in surge and sway. For the second model, the linearized mooring line model was replaced with the standard interface between FAST and the quasi-static mooring system module. To see how well these simpler models agreed with higher fidelity simulations, in the third model the rigid RNA and tower were replaced with a fully flexible ones and the variable-speed generator-torque and blade-pitch control systems were enabled.

The published results<sup>6</sup> of Wayman's frequency-domain study included mean and SDs of the Gaussian-distributed responses at a variety of sea states, wind speeds and water depths. All three of our models were compared with only one of Wayman's cases. The chosen case used winds roughly at rated (11.2 m s<sup>-1</sup>), a water depth of 200 m and the same wave conditions considered in the test of the wave-elevation time series. Steady unsheared winds were used in the first two models, but for the third model with an active control system, turbulent and sheared winds were used, with a mean hub-height speed of 11.2 m s<sup>-1</sup> and IEC category B turbulence. As before, the wind and waves were co-directional and aligned with the surge coordinate.

For each model, the probability densities were computed for the output of all but the first 30 s of a series of four 10,000 s simulations (i.e. just short of 3 h each), which used different random seeds for the stochastic waves. An aggregate of the four cases was constructed before computing the probability densities. The resulting histograms were plotted against the normal probability density functions derived from the means and

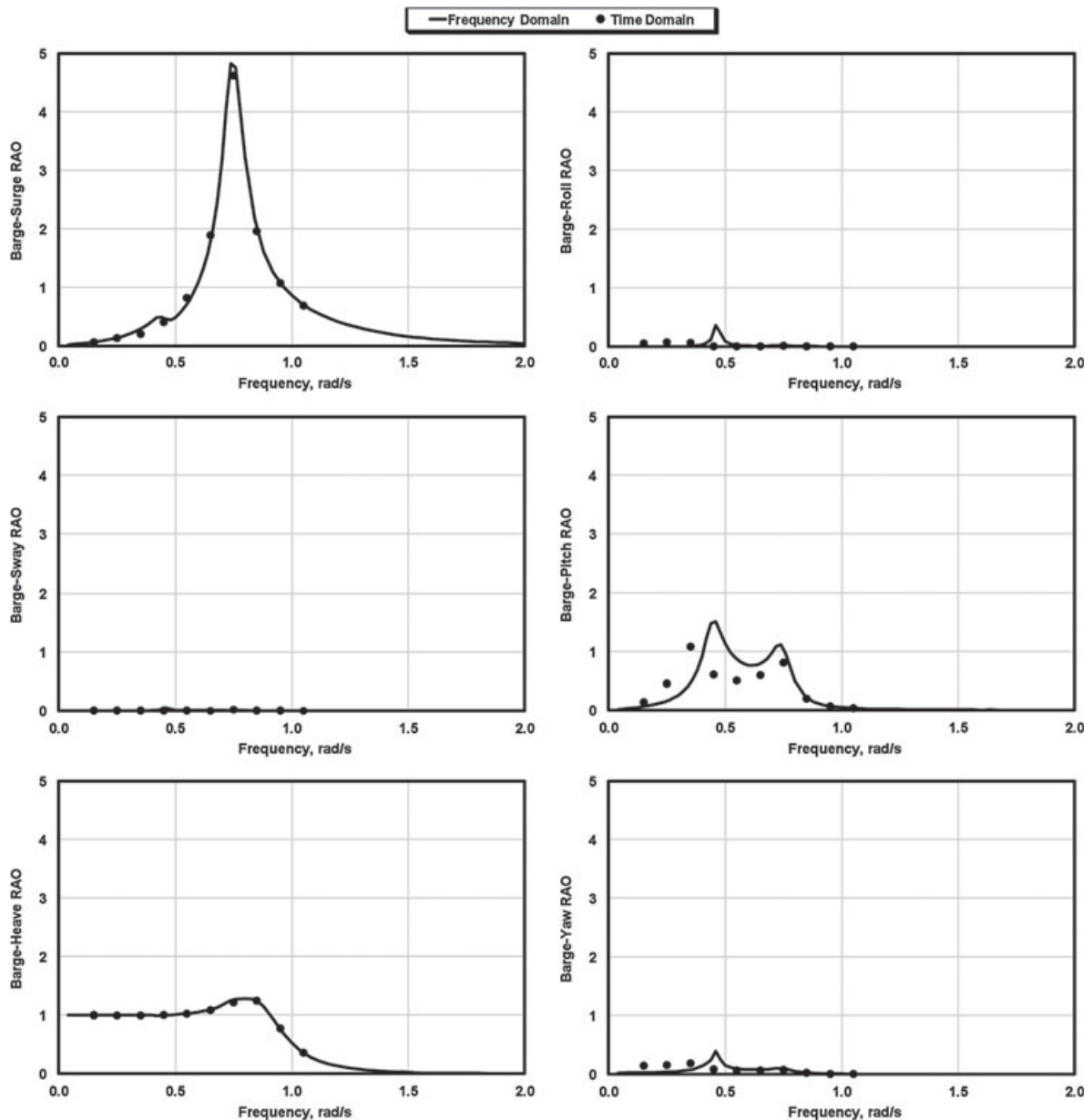


Figure 11. RAO comparisons for the MIT/NREL barge

standard deviations of Wayman's frequency-domain analysis<sup>6</sup> (the frequency-domain results of Wayman<sup>6</sup> were corrected by a factor of  $\sqrt{180/\pi}$  according to the error documented in Jonkman<sup>16</sup>).

Figure 12 presents the comparison between our time-domain results and Wayman's frequency-domain results. Because the differences between the results of our second and third models were much smaller than the changes brought about by the switch to nonlinear mooring lines, the figure shows the results from only the first and third models. As with the RAOs, the surge and heave predictions from the model with the linearized mooring lines agree very well. The spread for the pitch response is narrower for our simulation with the linearized mooring system than it is in Wayman's predictions. This is consistent with what the pitch RAO com-

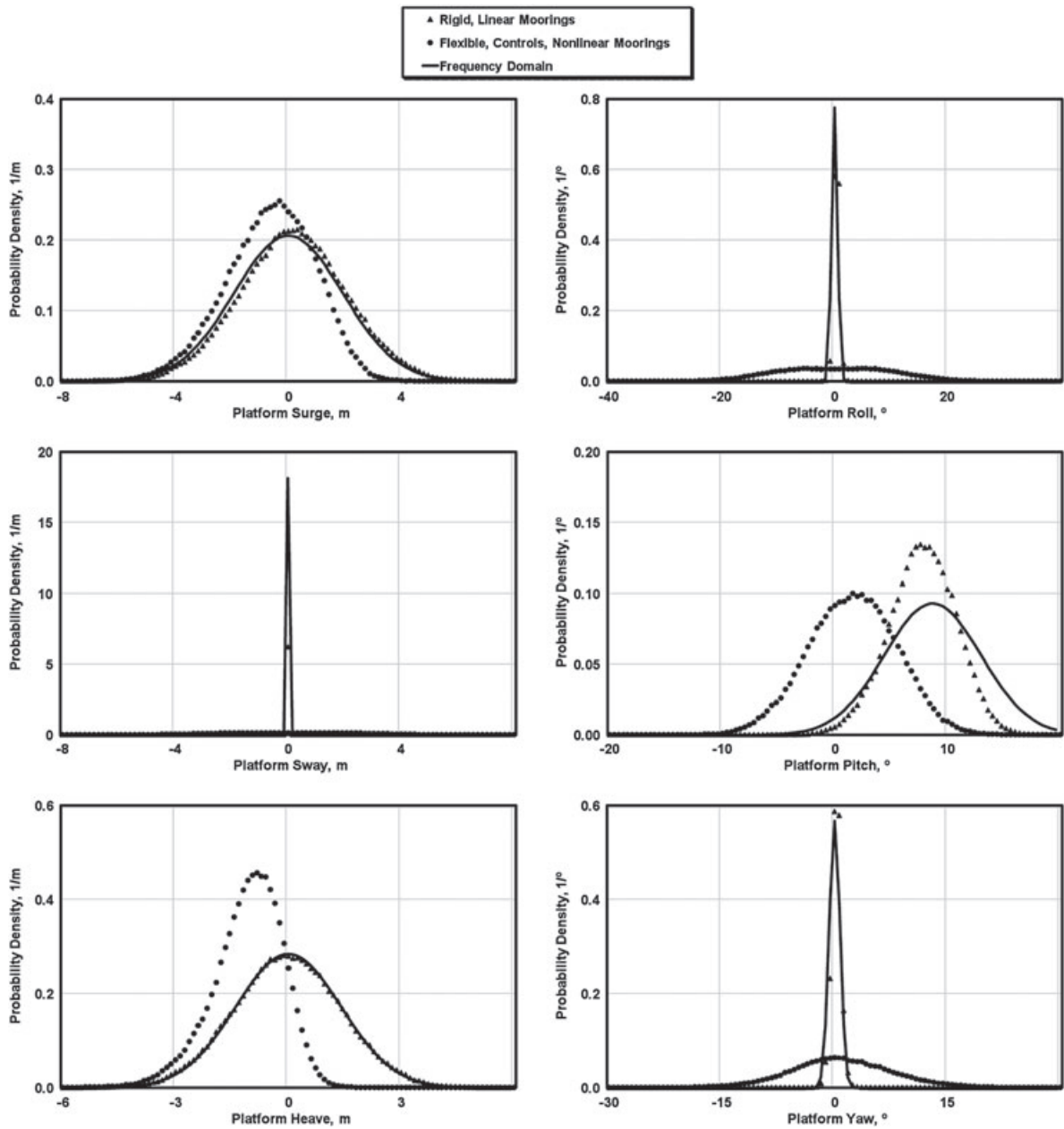


Figure 12. Probability density comparisons for the MIT/NREL barge

parison showed in Figure 11—that is, Wayman’s RAO was greater at  $0.429 \text{ rad s}^{-1}$  than the magnitude predicted by our model.

After introducing the non-linear mooring system module into the FAST simulations, the mean surge, pitch and heave responses decreased considerably (see Figure 12). This is because once the lines go taut, the stiffness increases dramatically and the mooring system essentially acts as a four-bar linkage. This keeps the platform from rising as high or from travelling as far downwind. The thrust on the rotor tries to pitch the turbine downwind, but the higher tensioned upwind mooring lines prevent the upwind end of the barge from

lifting so far out of the water; the platform, in turn, is pulled slightly upwind. Because there is more coupling in the system in the higher fidelity model, the spread of values for the sway, roll and yaw is also much greater than in the simpler model.

## Conclusions

The vast deepwater wind resource represents a potential to use offshore floating wind turbines to power much of the world with renewable energy. Before this research, many floating wind turbine concepts had been proposed, but few had or could have been evaluated with respect to their dynamics because available modelling capabilities were limited.

The limitations of previous time- and frequency-domain studies on offshore floating wind turbines motivated the development of simulation capability for modelling the fully coupled aero-hydro-servo-elastic response of such systems. This capability was developed by combining the computational methodologies of the land-based wind turbine and offshore O&G industries. The aero-servo-elastic land-based wind turbine simulation capability of FAST with AeroDyn and MSC.ADAMS with A2AD and AeroDyn were interfaced with the external hydrodynamic wave-body interaction program WAMIT. To establish these interfaces, modules were developed for treating time-domain hydrodynamics (HydroDyn) and quasi-static mooring system responses. The HydroDyn hydrodynamics module was developed to account for linear hydrostatic restoring; nonlinear viscous drag from incident-wave kinematics, sea currents and platform motion; the added-mass and damping contributions from linear wave radiation, including free-surface memory effects; and the incident-wave excitation from linear diffraction in regular or irregular seas. The quasi-static mooring line module was developed to account for the elastic stretching of an array of homogenous taut or slack catenary lines with seabed interaction. The simulation capability was developed with enough sophistication to address the primary limitations of the previous frequency- and time-domain studies. In addition, the simulation program has the features required to perform integrated loads analyses. To make it useful for examining the technical feasibility of a variety of offshore floating wind turbine concepts, the simulation capability was made universal enough to analyse a variety of RNA, tower, support platform and mooring system configurations.

Through model-to-model comparisons, the newly developed simulation capability was tested to ensure its correctness. Tests verified that the PSD and probability density of the wave-elevation record computed by HydroDyn matched the prescribed target spectrum and Gaussian distribution, respectively. It was demonstrated that WAMIT produces acceptable input for HydroDyn, and from this hydrodynamic input, HydroDyn was shown to correctly generate the radiation impulse-response functions. It was also shown that the quasi-static mooring system module correctly solves a classic benchmark problem for the static equilibrium of a suspended cable structure. In addition, the mooring system module was demonstrated to predict nonlinear force-displacement relationships consistent with an independent analysis. Finally, the results from the fully coupled time-domain analysis were shown to agree with results generated from a frequency-domain approach. The results of all the verification exercises were favourable and gave confidence to pursue more thorough investigations into the dynamic behaviour of offshore floating wind turbines.

## Acknowledgements

This work was performed at NREL in support of the US Department of Energy under contract number DE-AC36-99-GO10337 and in support of a Cooperative Research and Development Agreement (CRD-06-178) with ITI Energy.

## References

1. Musial W, Butterfield S. Future for offshore wind energy in the United States. *EnergyOcean Proceedings*, June 2004, Palm Beach, FL; NREL/CP-500-36313, NREL: Golden, CO.

2. Butterfield S, Musial W, Jonkman J, Sclavounos P, Wayman L. Engineering challenges for floating offshore wind turbines. *Copenhagen Offshore Wind 2005 Conference and Expedition Proceedings* 26–28 October, Copenhagen, 2005. (CD-ROM)
3. Passon P, Kühn M. State-of-the-art and development needs of simulation codes for offshore wind turbines. *Copenhagen Offshore Wind 2005 Conference and Expedition Proceedings*, 26–28 October, Copenhagen. Copenhagen, 2005. (CD-ROM)
4. Bulder, B. H., van Hees, Henderson, Huijsmans, Pierik, Sniijders, Wijnants, Wolf. Study to feasibility of and boundary conditions for floating offshore wind turbines. Novem 2002-CMC-R43, ECN, MARIN, Lagerway the Windmaster, TNO, TUD, MSC, December 2002.
5. Lee KH. Responses of floating wind turbines to wind and wave excitation. MS Thesis, Department of Ocean Engineering, MIT, Cambridge, MA, January 2005.
6. Wayman E. Coupled dynamics and economic analysis of floating wind turbine systems. MS Thesis, Department of Mechanical Engineering, MIT, Cambridge, MA, June 2006.
7. Vijfhuizen WJMJ. Design of a wind and wave power barge. MS Thesis, Department of Naval Architecture and Mechanical Engineering, Universities of Glasgow and Strathclyde, Glasgow, Scotland, September 2006.
8. Henderson AR, Patel MH. On the modelling of a floating offshore wind turbine. *Wind Energy* 2003; **6**:53–86.
9. Withee JE. Fully coupled dynamic analysis of a floating wind turbine system. PhD Thesis, Department of Ocean Engineering, MIT, Cambridge, MA, 2004.
10. Fulton GR, Malcolm DJ, Moroz E. Design of a semi-submersible platform for a 5 Mw wind turbine. *Proceedings of the 44th AIAA Aerospace Sciences Meeting and Exhibit*, 9–12 January, Reno, NV, 2006. (CD-ROM)
11. Zambrano T, MacCready T, Kiceniuk T Jr, Roddier DG, Cermelli CA. Dynamic modeling of deepwater offshore wind turbine structures in gulf of mexico storm conditions. *Proceedings of OMAE2006 25th International Conference on Offshore Mechanics and Arctic Engineering*, 4–9 June, Hamburg, Germany, 2006. (CD-ROM)
12. Nielsen FG, Hanson TD, Skaare B. Integrated dynamic analysis of floating offshore wind turbines. *Proceedings of OMAE2006 25th International Conference on Offshore Mechanics and Arctic Engineering*, 4–9 June, Hamburg, Germany, 2006. (CD-ROM)
13. Skaare B, Hanson TD, Nielsen FG. Importance of control strategies on fatigue life of floating wind turbines. *Proceedings of OMAE2007 26th International Conference on Offshore Mechanics and Arctic Engineering*, 10–15 June, San Diego, CA, 2007. (CD-ROM)
14. Zambrano T, MacCready T, Roddier DG, Cermelli CA. Design and installation of a tension moored wind turbine. *Proceedings of OMAE2007 26th International Conference on Offshore Mechanics and Arctic Engineering*, 10–15 June, San Diego, CA, 2007. (CD-ROM)
15. Larsen TJ, Hanson TD. A method to avoid negative damped low frequent tower vibrations for a floating, pitch controlled wind turbine. *Journal of Physics: Conference Series, The Second Conference on the Science of Making Torque From Wind*, Copenhagen, 28–31 August 2007; DOI: 10.1088/1742-6596/75/1/012073.
16. Jonkman JM. Dynamics modeling and loads analysis of an offshore floating wind turbine. PhD Thesis, Department of Aerospace Engineering Sciences, University of Colorado, Boulder, CO, 2007. [Online]. Available: <http://www.nrel.gov/docs/fy08osti/41958.pdf> (Accessed 25 February 2009)
17. Jonkman JM, Buhl ML Jr. *FAST User's Guide*, NREL/EL-500-38230 (previously NREL/EL-500-29798). NREL: Golden, CO, 2005.
18. Laino DJ, Hansen AC. *User's Guide to the Wind Turbine Dynamics Aerodynamics Computer Software AeroDyn*. Windward Engineering LLC: Salt Lake City, UT, 2002.
19. Laino DJ, Hansen AC. *User's Guide to the Computer Software Routines AeroDyn Interface for ADAMS®*. Windward Engineering LLC: Salt Lake City, UT, 2001.
20. Lee CH, Newman JN. *WAMIT® User Manual, Versions 6.3, 6.3PC, 6.3S, 6.3S-PC*. WAMIT, Inc.: Chestnut Hill, MA, 2006.
21. Greenwood DT. *Principles of Dynamics* (2nd edn). Prentice-Hall, Inc.: Englewood Cliffs, NJ, 1998.
22. Horn RA, Johnson CR. *Matrix Analysis*. Cambridge University Press, Cambridge, 1985.
23. Kane TR, Levinson DA. *Dynamics: Theory and Applications*. McGraw-Hill Inc.: New York, 1985.
24. Faltinsen OM. *Sea Loads on Ships and Offshore Structures*. Cambridge University Press: Cambridge, 1990
25. Newman JN. *Marine Hydrodynamics*. The MIT Press: Cambridge, MA, 1997.
26. Cummins WE. The impulse response function and ship motions, *Schiffstechnik* 1962; **9**:101–109.
27. Ogilvie TF. Recent progress toward the understanding and prediction of ship motions. *Fifth Symposium on Naval Hydrodynamics*, September, 1964, pp. 3–128.
28. Strum RD, Kirk DE. *Contemporary Linear Systems Using MATLAB®*. Brooks/Cole: Pacific Grove, CA, 2000.
29. Swarztrauber PN. FFTPACK, NCAR's mathematical and statistical libraries online database. [Online]. Available: <http://www.cisl.ucar.edu/softlib/FFTPACK.html> (Accessed 12 July 2007)
30. Rubinstein RY. *Simulation and the Monte Carlo Method*. John Wiley & Sons, Inc: New York, 1981: 86–91.
31. Wehausen JV. Initial-value problem for the motion in an undulating sea of a body with fixed equilibrium position. *Journal of Engineering Mathematics* 1967; **1**:1–17.

32. Jonkman BJ, Buhl ML Jr. *TurbSim User's Guide*, NREL/EL-500-41136. NREL: Golden, CO, 2007.
33. Jonkman J, Butterfield S, Musial W, Scott G. Definition of a 5-MW reference wind turbine for offshore system development, NREL/TP-500-38060, NREL: Golden, CO, 2009.
34. Jonkman JM. Modeling of the UAE wind turbine for refinement of FAST\_AD. MS Thesis, Department of Mechanical Engineering, CSU, Fort Collins, CO, 2001.
35. Jonkman JM, Buhl ML Jr. New developments for the NWTTC's FAST aeroelastic HAWT simulator. *A Collection of the 2004 ASME Wind Energy Symposium Technical Papers Presented at the 42nd AIAA Aerospace Sciences Meeting and Exhibit*, 5–8 January 2004, Reno, NV, AIAA-2004-0504, AIAA: Reston, VA, ASME: New York, January 2004, pp. 181–191; NREL/CP-500-35077 (and NREL/CP-500-36501), NREL: Golden, CO.
36. Majock A. Evaluation report: Design codes FAST and ADAMS® for load calculations of onshore wind turbines. *Report No. 72042*, Germanischer Lloyd WindEnergie GmbH: Hamburg, Germany, May 26, 2005.
37. Underwood PG. Dynamic relaxation. *Computational Methods for Transient Analysis* 1983; **1**:245–265.